ABSTRACT

ALLEN, ZACHARY. Design and Characterization of a Ground State Analog of a Charge-Separated Excited State. (Under the direction of Dr. David A. Shultz)

Presented herein is the synthesis and characterization of a novel donor-acceptor ground state analog for Electron Spin Polarization (ESP). Following an introduction to ESP and a discussion of previous work that is relevant to this project, the synthesis of a Pt(II) complex with a verdazyl (VDZ) acceptor and catecholate (CAT) donor is discussed. Electronic absorption spectroscopy results reveal a charge-separated excited state with a closed-shell radical acceptor ($VDZ^{\bullet -}$) and an open-shell semiquinone ($SQ^{\bullet +}$) donor with the CAT → VDZ LL`CT transition near 10,000 cm^{-1}. Electron Paramagnetic Resonance (EPR) experiments reveal a spectrum with little hyperfine structure except that of a ^{195}Pt hyperfine of 43 G and a g-value of 2.019. Following characterization of the ground state VDZ-Pt-CAT complex, attempts at oxidation to $[VDZ\text{-}Pt\text{-}SQ]^{+}$ are discussed.

Design and Characterization of a Ground State Analog of a Charge-Separated Excited State

By

Zachary Allen

A thesis submitted to the Graduate Faculty of North Carolina State University in partial fulfillment of the requirements of the Degree of Master of Science.

Chemistry

Raleigh, North Carolina

2022

APPROVED BY:

_____

Dr. David Shultz

Committee Chair

_____ _____

Dr. Felix Castellano Dr. Vincent Lindsay

BIOGRAPHY

Zachary Allen was born in Greensboro, NC to his parents Mark and Keisha Allen and was raised in Greensboro along with his two brothers. Zack and his brothers were homeschooled by his maternal grandmother who taught them to read and write. With some help from his Uncle David, Zack fell in love with reading and became an avid reader which continues to the present day.

Following high school graduation, Zack attended the University of North Carolina at Greensboro. During his undergraduate years, he conducted research in the Petersen group of the Department of Chemistry and Biochemistry where he realized his passion for chemistry. In addition to studying chemistry, Zack studied both philosophy and classical studies and earned minors in both. Upon graduating, he decided to pursue graduate studies at North Carolina State University where he met Dr. David Shultz and Patrick Hewitt (now Dr. Hewitt) and let them talk him into studying very complicated chemistry. After two and a half years of research, Zack wrote and successfully defended his Master`s Thesis.

TABLE OF CONTENTS

APPENDICES

LIST OF FIGURES

LIST OF TABLES

LIST OF SCHEMES

Chapter I: Electron Spin Polarization and Related Work

I.1 Quantum Information Science and Electron Spin Polarization

Electron spin polarization (ESP) deals with the manipulation of one of the most basic building blocks of chemistry: the electron. An English physicist by the name of J. J. Thompson was credited with the discovery of the electron with his cathode ray tube experiments at the end of the 19th century.[1] However, it was approximately 20 years later when Gilbert Lewis brought forward the concept of electrons in pairs that the fundamentals for rationalizing molecular geometry, bonding and reactivity that are still discussed today, were born.[2] The basic unit of the electron pair became crucial to understanding the electronic structure of molecules. In present times, the electron pair is better understood through the application of the Pauli exclusion principle which imposes a requirement of antisymmetrization on the wave function when applied to two electrons with measurable spin possibilities.[2] It is the concept of an electron pair and the rules that govern it that allow the discovery of new mechanisms for electron spin polarization that can be used in new and exciting fields of science. A chemist`s ability to design and manipulate molecular systems presents untold possibilities for Quantum Information Science (QIS). The field of QIS relies on exploiting the intrinsic quantum nature of matter and photons by taking advantage of the two quantum properties of superposition and entanglement of quantum states.[3] Research that displays the exploitation and manipulation of these properties is of great importance to furthering QIS as a whole.

In the simplest form, spin polarization can be thought of as a phenomenon where one spin is favored over the other by some influencing factor. The complexity is added when molecular structure-property relationships that determine the preference are explored and elucidated. Less

challenging examples of such factors include the Pauli exclusion principle and Hund's Rules which govern the relative orientation (spin "up" or spin "down") and occupation order of orbital sublevels. Further searching will provide an abundance of information pertaining to complex spin polarization mechanisms discovered through years of research.[4,5] Yet, even with the increasing interest in investigating spin polarizing phenomenon and, more broadly, QIS related fields, there has been little information published regarding strategies for designing molecular systems that deal with ultrafast optical generation,[6] initiation[6] or coupling[7] of quantum spin qubits. With this in mind, the work presented herein reveals the design of a parent chromophore that can serve as the core for a molecular system that can be synthetically manipulated to great effect with regards to controlling the photomanipulation of quantum spin qubits. The engineering of this chromophore and its future potential is based on years of Shultz Group research dealing with electron spin polarization, chromophore engineering and complex data acquisition and analysis.

I.2 Donor-Acceptor Motif

The donor-acceptor motif shown in Figure I.1 has been used to great effect in studying ligand control of the excited state lifetimes of certain donor-acceptors complexes[8] and inducing ground state spin polarization through excited state spin entanglement[9] by the Shultz group and collaborators. The (dithiolene)Pt(diimine) series of compounds generates interest due to its photophysical properties and flexible electronic structure.[8] However, the most interesting aspect of this molecular system from the perspective of this project is the excited state donor → acceptor ligand-to-ligand charge transfer (LL`CT) transition. Research shows that this transition occurs in the visible-to-near-infrared (NIR) region and is characteristic of these complexes.[8] To

take advantage of this transition which is characteristic to these square planar, d^8 Pt(II) complexes, a similar donor-acceptor structural motif was implemented.

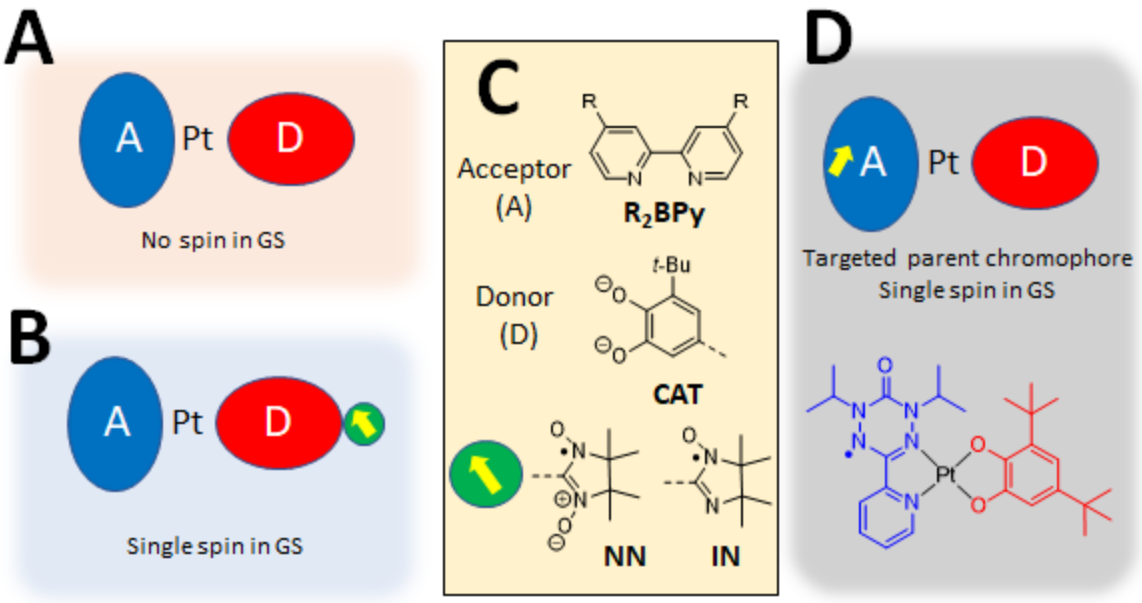

Figure I.1: Donor-Acceptor ground state structural layouts. **A**: Donor-Acceptor system with no ground state (GS) spins. **B**: Donor-Acceptor system with uncorrelated spin in the GS. **C**: Examples of acceptors (A), donors (D) and stable radicals. **D**: Proposed donor-acceptor chromophore.

Referencing this work[8] further, the donor for this new donor-acceptor system will need to be chosen carefully. If this chromophore and future synthetic derivations will be used to probe electron spin polarization, excited state lifetimes shorter than the electron spin longitudinal relaxation time will be conducive to manipulating or entangling the spins.[9,10] Comparisons of dichalcogenolenes shown in Figure I.2 revealed that the 3,5-di-*tert*-butylcatecholate has the fastest LL`CT excited state decay rate among the tested dichalcogenolenes due to its rapid rate of internal conversion (k_{IC}) via back-electron transfer and slow intersystem crossing (k_{ISC}) caused by the symmetry forbidden $S_1 \rightarrow T_1$ transition.[8] With this in mind, the 3,5-di-*tert*-butylcatecholate will serve as the best choice for the donor.

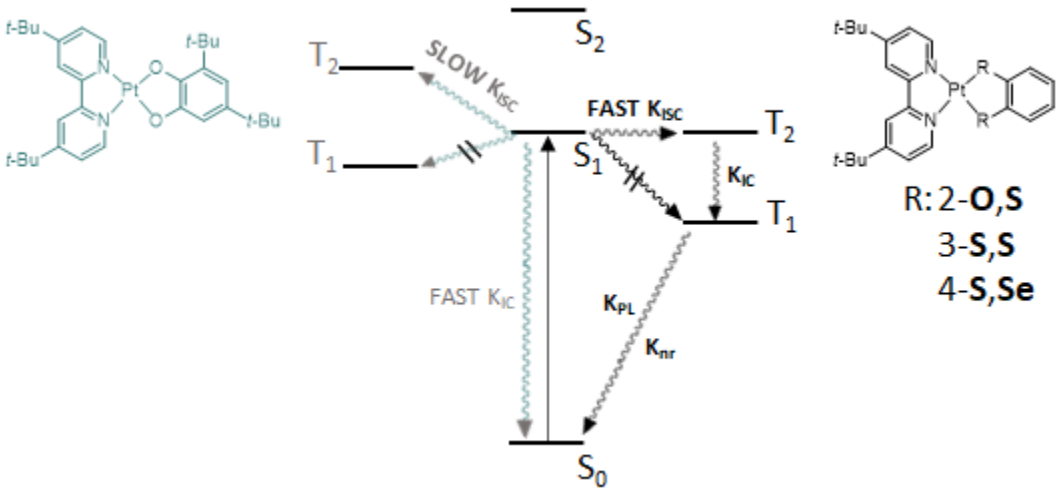

Figure I.2: Jablonski diagram for the photoprocesses that were observed for select dichalcogenolenes.[8]

Shown in Figure I.1 **A** and **B** are the ground states of previously reported donor-acceptor systems.[8–11] A common feature with both is the use of a diimine (bpy) bidentate ligand. Construction of a new molecular layout required the use of a new ligand, preferably one that had been previously investigated with published results establishing a robust synthetic scheme. Furthermore, to develop a system that can be used to accomplish the goals for understanding the electronic structure of the excited states involved in photoinduced electron spin polarization of the recovered ground state, a stable radical acceptor will be needed. Hicks has reported the preparation and characterization of a paramagnetic bpy analog that provides both synthetic rigor as well as intriguing electronic structure in the form of an oxoverdazyl.[12,13] This verdazyl, which is seen in Figure I.1 **D** as the acceptor, will vary from the existing work with the bipyridine acceptor due to the ground state acceptor containing spin. Upon photoexcitation, the previously reported work will form a (bpy$^{\bullet-}$)Pt(SQ) LL`CT excited state having open-shell donor-acceptor biradical character.[8] This work presented herein differs in that the LL`CT excited state will involve the CAT → VDZ CT which will effectively fill the "radical hole" of the VDZ and place

the spin on the donor side of the Pt(II) complex. For a one-spin system as shown in Figure I.1 **D**, that would form a (diimine^{-})Pt(SQ) LL`CT state where the VDZ would become a closed-shell radical and have a delocalized negative charge and the SQ would become an open-shell radical and carry a positive charge as well as the spin. In such a system, there is no influence to initiate spin polarization; however, if this system was used with a donor with an appended radical as shown in Figure I.1 **B**, photo-initiation of spin polarization may be possible. Such factors involve the use of bridge-specific CAT derivations probed by the Shultz group in previous donor-bridge-acceptor biradicals.[14,15]

In addition, the observed photoinduced spin polarization reported in our series of papers requires fast excited state equilibration of m_s-levels, the rates of which are proportional to zero-field splitting (ZFS) of the excited state spin quartet. This ZFS is in turn related to that of the chromophoric triplet state which is not observed spectroscopically. Thus, a ground state analog of the chromophoric excited triplet state is desired in order to measure relevant ZFS parameters.

I.3 Controlling Ground State ESP via Excited State Exchange Interactions

Peripherally elaborated radical systems exhibit ground state spin polarization through photoexcited state exchange-coupled, multi-spin entanglement.[9,11] Designing a one-spin, radical acceptor-based precursor is meant to build upon this work and further produce novel chromophores where photomanipulation of spin qubits will be possible. Such radical elaborated donor-acceptor systems will further our understanding of ultrafast optical generation and coupling of spin qubits as well as show how robust synthetic strategies can be implemented to influence coupled molecular spin qubits. To exploit the VDZ-Pt-CAT complex shown in Figure I.1 **D** for electron spin polarization, the donor half of the complex would need further elaboration

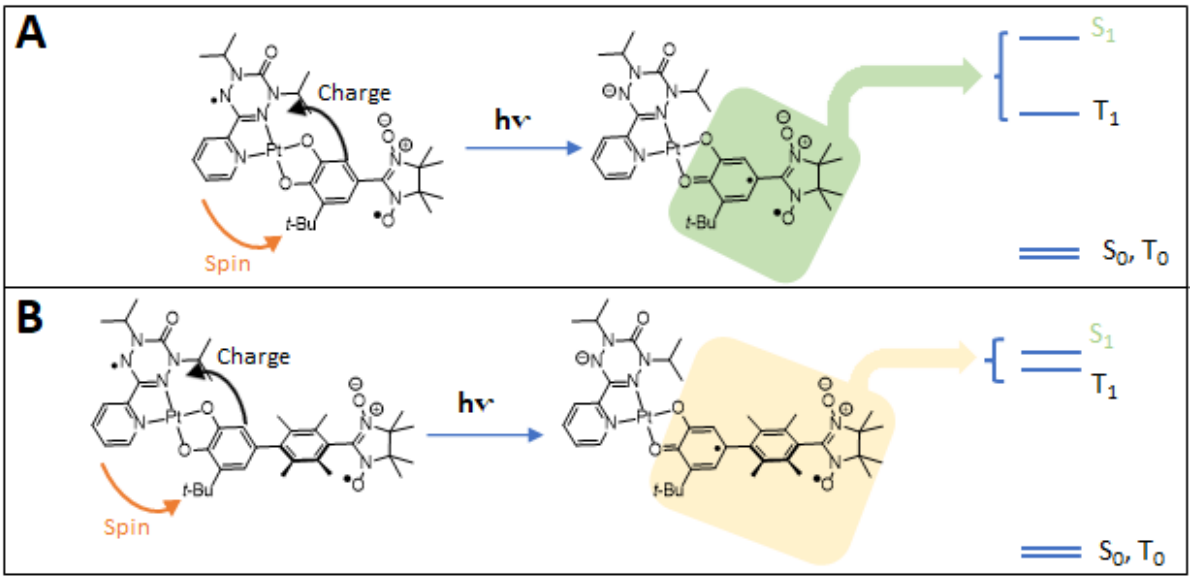

Figure I.3: Simplified diagram showing the effects on the singlet-triplet gap when changing the CAT donor.

with the addition of a charge separated stable radical. Recent Shultz group work with (bpy)Pt(CAT-bridge-NN) complexes have provided insight into ground state electron spin polarization through excited state exchange interactions that can be applied by changing the 3,5-di-*tert*-butylcatechol to the corresponding CAT-NN or CAT-bridge-NN ligand. Shown in Figure

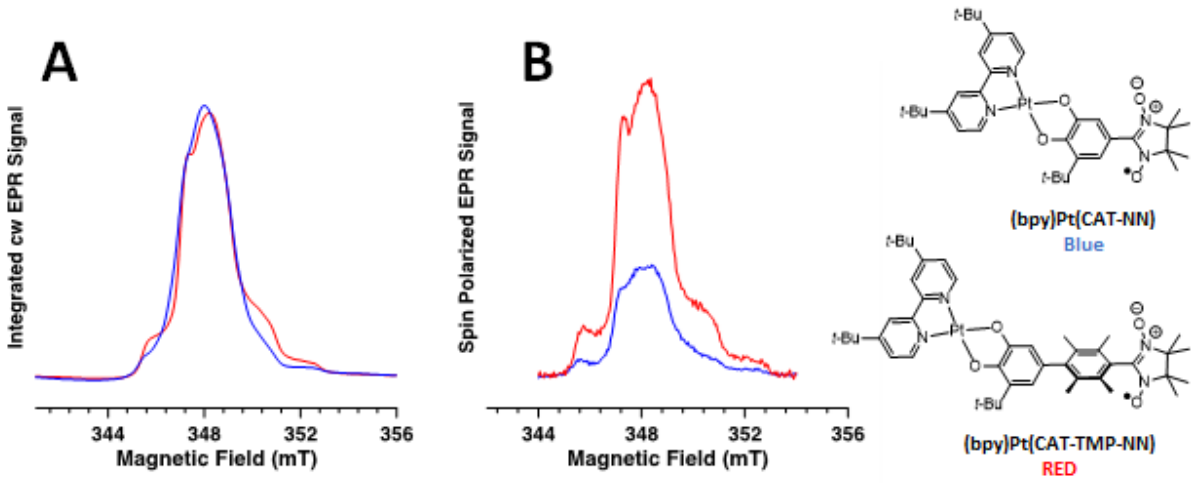

Figure I.4: X band EPR of (bpy)Pt(CAT-NN) (blue lines) and (bpy)Pt(CAT-TMP-NN) (red lines) in 2-MTHF at 20 K.[10] **A**: ground state cw-EPR without photoexcitation. **B**: Photo-induced, spin-polarized TREPR spectra.

I.3 is a simplified diagram that displays how altering the radical appended CAT donor can influence the relative energies of the excited state manifold. This is based on recently published work using (bpy)Pt(CAT-bridge-NN) complexes with results shown in Figure I.4.[11] Shown in Figure I.4 **A** is the continuous wave EPR (cw-EPR) spectra involving the aforementioned CAT donors in the ground state in frozen solution at 20 K before light-induced excitation. Following the application of light, we see a light-induced, spin-polarized time-resolved EPR (TREPR) signal from both the CAT-NN and the CAT-TMP-NN complexes in Figure I.4 **B**. It is observed that both CAT-NN and CAT-TMP-NN produce ground state ESP, though of differing magnitudes. The magnitude is affected by the bond torsions caused by the TMP bridge of the

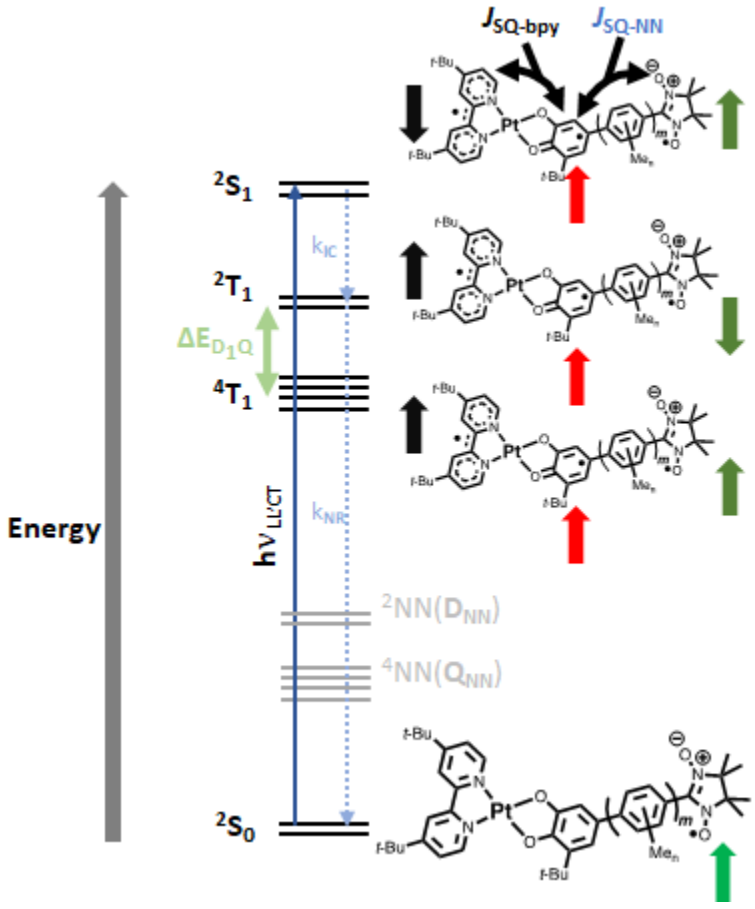

Figure I.5: Excited State Manifold

CAT-TMP-NN which affects the excited state exchange interaction ($\boldsymbol{J}_{SQ\text{-}NN}$). Previous work with Zn(II) complexes with biradical ligands provides estimates of $\boldsymbol{J}_{SQ\text{-}NN}$ by imitating the donor half of the LL`CT excited states.[14]

Light-induced excitation of (bpy)Pt(CAT-NN) gives a (bpy$^{\bullet-}$)Pt(SQ-B-NN) with there either being no bridge or TMP. Upon excitation to the $^2S_1$ state, there is rapid internal conversion to $^2T_1$ followed by an equilibration of $^2T_1$ and $^4T_1$ which is shown as ΔE_{D1Q} in Figure I.5. The bridge modulates the $\boldsymbol{J}_{SQ\text{-}NN}$ which determines the energy gap between the excited quartet and doublet states (ΔE_{D1Q}).[11] Following equilibration, $^2T_1$ is polarized and rapid non-radiative decay transmits a non-Boltzmann population to the ground state through the Reversed Quartet Mechanism (RQM) shown in Figure I.6.[4,16] Shown in Figure I.6 **A** is the RQM and the resulting

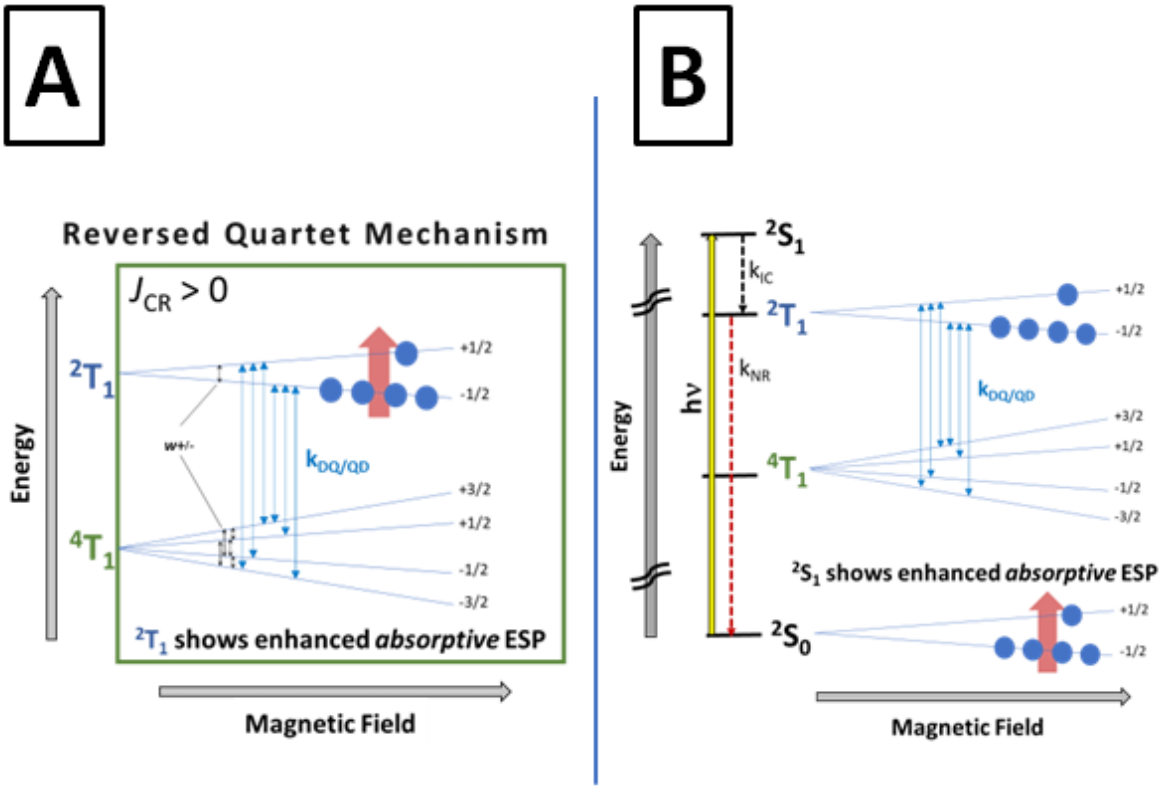

Figure I.6: A: the Reversed Quartet Mechanism. B: Depiction of the ESP transmitted from the ES to the GS.

polarization of the $^2T_1$ level. That polarization is then transmitted to the ground state $^1S_0$ which is shown in Figure I.6 **B**.

The work presented[9,11] represents one way of utilizing the VDZ-Pt-CAT complex designed in this project in future endeavors. Controlling the ground state ESP through excited state exchange interactions has already been investigated with other diimine acceptors. These systems use the same donor-acceptor motif to accomplish the ground state ESP. The novelty of using the VDZ-Pt-CAT will come in the form of making previously unreported complexes that will form a closed shell radical acceptor that will have the hole on the CAT donor as the paramagnetic VDZ is quenched. These charge transfer complexes could provide valuable insight into the mechanisms of ground state ESP as well as further develop the photomanipulation of spin qubits in quantum systems. In addition, the spin Hamiltonian parameters of $[VDZ\text{-}Pt\text{-}SQ]^+$ will elucidate the factors affecting the excited state $^2T_1$ - $^4T_1$ equilibration that is the source of the spin polarization.

I.4 References

(1) Tro, N. *Chemistry: A Molecular Approach*, 2nd ed.; Dan Kaveney, 2011.

(2) Bader, R. F. W.; Johnson, S.; Tang, T. H.; Popelier, P. L. A. The Electron Pair. *J. Phys. Chem.* **1996**, *100* (38), 15398–15415. https://doi.org/10.1021/jp961297j.

(3) Wasielewski, M. R.; Forbes, M. D. E.; Frank, N. L.; Kowalski, K.; Scholes, G. D.; Yuen-Zhou, J.; Baldo, M. A.; Freedman, D. E.; Goldsmith, R. H.; Goodson, T.; Kirk, M. L.; McCusker, J. K.; Ogilvie, J. P.; Shultz, D. A.; Stoll, S.; Whaley, K. B. Exploiting Chemistry and Molecular Systems for Quantum Information Science. *Nat. Rev. Chem.* **2020**, *4* (9), 490–504. https://doi.org/10.1038/s41570-020-0200-5.

(4) Rozenshtein, V.; Berg, A.; Stavitski, E.; Levanon, H.; Franco, L.; Corvaja, C. Electron Spin Polarization of Functionalized Fullerenes. Reversed Quartet Mechanism. *J. Phys. Chem. A* **2005**, *109* (49), 11144–11154. https://doi.org/10.1021/jp0540104.

(5) McLauchlan, K. A. Physical Chemistry through Electron Spin Polarisation. The Bruker Lecture. *J. Chem. Soc. Perkin Trans. 2* **1997**, No. 12, 2465–2472. https://doi.org/10.1039/a702507f.

(6) Olshansky, J. H.; Krzyaniak, M. D.; Young, R. M.; Wasielewski, M. R. Photogenerated Spin-Entangled Qubit (Radical) Pairs in DNA Hairpins: Observation of Spin Delocalization and Coherence. *J. Am. Chem. Soc.* **2019**, *141* (5), 2152–2160. https://doi.org/10.1021/jacs.8b13155.

(7) Timco, G. A.; Carretta, S.; Troiani, F.; Tuna, F.; Pritchard, R. J.; Muryn, C. A.; McInnes, E. J. L.; Ghirri, A.; Candini, A.; Santini, P.; Amoretti, G.; Affronte, M.; Winpenny, R. E.

P. Engineering the Coupling between Molecular Spin Qubits by Coordination Chemistry. *Nat. Nanotechnol.* **2009**, *4* (3), 173–178. https://doi.org/10.1038/nnano.2008.404.

(8) Yang, J.; Kersi, D. K.; Giles, L. J.; Stein, B. W.; Feng, C.; Tichnell, C. R.; Shultz, D. A.; Kirk, M. L. Ligand Control of Donor-Acceptor Excited-State Lifetimes. *Inorg. Chem.* **2014**, *53* (10), 4791–4793. https://doi.org/10.1021/ic500217y.

(9) Kirk, M. L.; Shultz, D. A.; Hewitt, P.; Stasiw, D. E.; Chen, J.; van der Est, A. Chromophore-Radical Excited State Antiferromagnetic Exchange Controls the Sign of Photoinduced Ground State Spin Polarization. *Chem. Sci.* **2021**, *12* (41), 13704–13710. https://doi.org/10.1039/d1sc02965g.

(10) Kirk, M. L.; Shultz, D. A.; Chen, J.; Hewitt, P.; Daley, D.; Paudel, S.; Van Der Est, A. Metal Ion Control of Photoinduced Electron Spin Polarization in Electronic Ground States. *J. Am. Chem. Soc.* **2021**, *143* (28), 10519–10523. https://doi.org/10.1021/jacs.1c04149.

(11) Kirk, M. L.; Shultz, D. A.; Hewitt, P.; Van Der Est, A. Excited State Exchange Control of Photoinduced Electron Spin Polarization in Electronic Ground States. *J. Phys. Chem. Lett.* **2022**, *13* (3), 872–878. https://doi.org/10.1021/acs.jpclett.1c03491.

(12) Johnston, C. W.; McKinnon, S. D. J.; Patrick, B. O.; Hicks, R. G. The First "Kuhn Verdazyl" Ligand and Comparative Studies of Its PdCl2 Complex with Analogous 6-Oxoverdazyl Ligands. *Dalt. Trans.* **2013**, *42* (48), 16829–16836. https://doi.org/10.1039/c3dt52191e.

(13) McKinnon, S. D. J.; Gilroy, J. B.; McDonald, R.; Patrick, B. O.; Hicks, R. G. Magnetostructural Studies of Palladium(Ii) and Platinum(Ii) Complexes of Verdazyl

Radicals. *J. Mater. Chem.* **2011**, *21* (5), 1523–1530. https://doi.org/10.1039/c0jm02560g.

(14) Kirk, M. L.; Shultz, D. A.; Stasiw, D. E.; Lewis, G. F.; Wang, G.; Brannen, C. L.; Sommer, R. D.; Boyle, P. D. Superexchange Contributions to Distance Dependence of Electron Transfer/Transport: Exchange and Electronic Coupling in Oligo(Para-Phenylene)- and Oligo(2,5-Thiophene)-Bridged Donor-Bridge-Acceptor Biradical Complexes. *J. Am. Chem. Soc.* **2013**, *135* (45), 17144–17154. https://doi.org/10.1021/ja4081887.

(15) Hewitt, P.; Shultz, D. A.; Kirk, M. L. Rules for Magnetic Exchange in Azulene-Bridged Biradicals: Quo Vadis? *J. Org. Chem.* **2021**, *86* (21), 15577–15587. https://doi.org/10.1021/acs.joc.1c02085.

(16) Tripathi, A. K.; Rane, V.; Kundu, S.; Das, R. A Phenomenological Scheme for Reversed Quartet Mechanism of Electron Spin Polarization in Covalently Linked Systems of Chromophore and Free Radical: Determination of Magnitude of Polarization and Application to PyreneO Linked Molecules. *J. Chem. Phys.* **2019**, *151* (15). https://doi.org/10.1063/1.5124731.

Chapter II. Synthetic Strategies for VDZ-Pt-CAT

II.1 Verdazyl Introduction

In the early 1960s, Kuhn and Trischmann discovered what would become the verdazyl class of stable organic radicals.[1] They attempted alkylation of formazans to give what they expected would be *N*-alkylated formazans but instead found that the intermediates would rearrange and give tetrazines in certain cases. These tetrazines could then be aerobically oxidized to give the verdazyl compounds.[2] Fast-forward to the present and a basic literature review will yield a plethora of completed and ongoing research of verdazyls. The interest in verdazyl compounds stems from the fact that they are spin-delocalized π radicals, aerobically and anaerobically stable and exhibit paramagnetic behavior.[3] These characteristics make them attractive targets for constructing magnetic materials.[2,3]

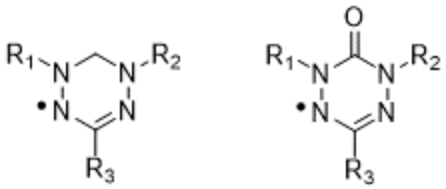

Figure II.1: The two classes of verdazyls.

Verdazyl radicals can be classified in to one of two classes: Kuhn verdazyls and oxoverdazyls. As shown in Figure II.1, the difference between the two classes of verdazyls is the carbon substitution between R_1 and R_2. The oxoverdazyl contains the carbonyl in that position while the Kuhn verdazyl contains a sp^3 hybridized carbon atom. Synthetically, the approaches can vary greatly depending on the R groups and whether the Kuhn or oxoverdazyl structure is desired.

II.2 Verdazyl Ligand Synthesis

Synthesis of the targeted verdazyl ligand, 1,5-di-*iso*-propyl-3-pyridin-2-yl-6-oxoverdazyl (VDZ), is well documented in the literature.[4–6,6–11] While starting from hydrazine (H_2NNH_2) and installing a boc-protecting group is possible,[12] the product of that reaction is also commercially available and was therefore purchased as the starting material for the synthetic route. The first reaction in Scheme II.1 is the condensation of the boc-protected hydrazine and acetone.

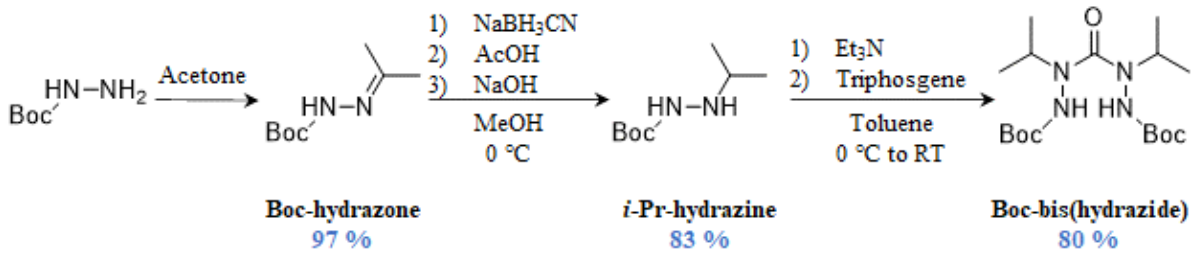

Scheme II.1: Synthetic route from the boc-protected hydrazine to the di-*tert*-butyl-2,2′-carbonylbis-(2-isopropylhydrazine-carboxylate).

The most important conditions for this reaction are maintaining a temperature of 25°C and ensuring that an excess of acetone is present for the duration of the reaction. Cooling the reaction will result in a decreased yield and heating the reaction can cause the acetone to evaporate. A 10-fold excess of acetone is used to help offset the loss of acetone by evaporation. The reaction yields *tert*-butyl-2-isopropylhydrazonecarboxylate (Boc-hydrazone) in high purity, but THF and hexanes can be used for recrystallization if needed.

Following the condensation, *tert*-butyl-2-*iso*-propylhydrazinecarboxylate (*i*-Pr-hydrazine) was made by reducing the boc-hydrazone with sodium cyanoborohydride in glacial acetic acid. The reaction was quenched using 6 M NaOH, followed by an aqueous workup to give *i*-Pr-hydrazine. Purification after the workup is typically unnecessary but can be carried out using

recrystallization with THF and hexanes or sublimation. Previous literature methods had resulted in a mixture of *i*-Pr-hydrazine and the cyanoborane adduct.[13] Pare and coworkers then found that a workup using 1 M KOH directly gave the product as a white solid.[13] This procedure was used for the synthetic route presented in Scheme II.1, but with slight variations. Utilizing the literature procedures[7,13], yields in the 50 % range were obtained. Changing to inert conditions and using dry methanol and 6 M NaOH for the workup increased yields to the 80-85 % range.

Initial reaction conditions reported for the synthesis of di-*tert*-butyl-2,2′-carbonylbis-(2-isopropylhydrazine-carboxylate) (Boc-bis-hydrazide) involved the use of the very toxic chemical phosgene.[13] However, it was later determined that triphosgene and triethylamine could be used in place of phosgene.[4] While phosgene and triphosgene share the same toxicity, triphosgene is a solid at room temperature whereas phosgene is a gas. This difference makes it easier to weigh out and scale up reactions. Triphosgene will undergo decomposition due to reaction intermediates which will facilitate a mild release of phosgene. This milder release of phosgene reportedly resulted in higher yields.[4]

In the synthesis of boc-bis(hydrazide), *i*-Pr-hydrazine and freshly distilled triethylamine were dissolved in dry toluene in inert conditions and cooled to 0 ℃. A separate solution containing the triphosgene in dry toluene was then transferred via cannula to the cool *i*-Pr-hydrazine solution while maintaining vigorous stirring. Copious amounts of triethylamine hydrochloride are formed during the addition of the triphosgene solution. If the reaction does not have vigorous stirring, a layer of the salt will form on the top of the solvent which will prevent the triphosgene solution from reaching the other reagents as it is added dropwise. After addition, the reaction was left to warm to room temperature for 18 hours. By keeping an inert atmosphere and using dry toluene and freshly distilled triethylamine, detrimental decomposition of the

triphosgene was minimized. Recall that the aim is for a mild phosgene release due to decomposition of the triphosgene from interactions with the starting materials. Moisture and triethylamine have undesired effects on triphosgene which will affect the yield.[4] After approximately 18 hours, the triethylamine hydrochloride salt is filtered and washed with warm toluene and then discarded. The filtrate is then concentrated and washed with heptane. Recrystallization using heptane is possible, but it was found that simply washing with heptane gave the desired purity due to the starting material being soluble in heptane at room temperature. Following established procedures[4,13] theses steps gave yields of 49-55 % while the highest

Table II.1: Reaction conditions for the synthesis of boc-bis(hydrazide).

Entry	Time (hrs.)	Solvent	Yield (%)
1	1	Toluene	20
2	2	Toluene	49
3	18	Toluene	85

reported yield was 74 %.[4] By increasing the amount of time for the reaction after the addition of the triphosgene solution, the yield was increased to 80-85 % as seen in Table II.1. In addition to increasing the time, the reaction remained in the ice bath as it slowly warmed to room temperature as opposed to removing the ice bath immediately after the addition.

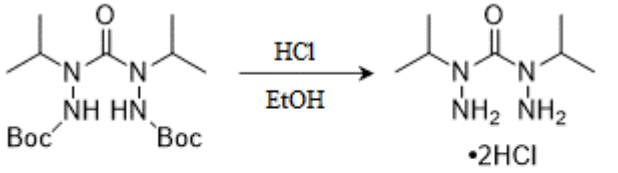

Boc-bis(hydrazide) **Bis(hydrazide) Salt**
< 97 %

Scheme II.2: Deprotection of the boc-bis(hydrazide).

The deprotection of the boc-bis(hydrazide) to the bis(hydrazide) salt was achieved following literature precedent as shown in Scheme II.2.[13,14] The removal of the boc-protecting

groups requires an excess of 37 % HCl in ethanol and gives a quantitative yield. An initial heating to 50 ℃ for 30 minutes aids deprotection but is not required. A mild effervescence due to the loss of CO_2 is observed during the reaction and can serve as a visual indicator for the decomposition of the boc-protecting groups. Following deprotection, the reaction is concentrated under reduced pressure to remove the excess HCl and ethanol to give the desired bis(hydrazide) salt. The product can be used without further purification but can be recrystallized from n-butanol if needed. The bis(hydrazide) salt has a sticky consistency without recrystallization but ^{1}H NMR shows that even without recrystallization, the product contains no noticeable impurities. Using the bis(hydrazide) salt without further purification gave no noticeable difference in yield for the next reaction.

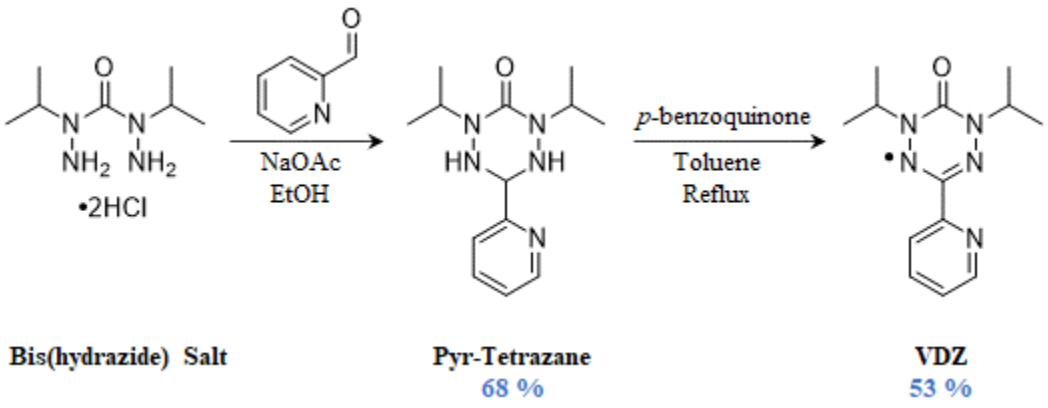

Scheme II.3: Formation and oxidation of the tetrazane ring structure.

With the boc-protecting groups removed, the tetrazane ring structure can be formed. After dissolving the bis(hydrazide) salt and 2-pyridinecarboxaldehyde in minimal ethanol, a solution containing sodium acetate dissolved in minimal ethanol is added and the reaction is left stirring for 24 hours. Upon completion, the reaction mixture is filtered, concentrated and the precipitate recrystallized from heptane. The use of dry ethanol in inert conditions did not significantly increase the yield as shown in Table II.2. In efforts to increase the yield, the base and solvent were changed to potassium carbonate and methanol. This change did not produce an

increase in yield but did produce an overall cleaner reaction. Utilizing the potassium carbonate and dry methanol gives a crude product that is easier to recrystallize from heptane.

Table II.2: Pyr-tetrazane reaction solvents and bases.

Entry	Time (hrs)	Solvent	Base	Yield (%)
1	5	EtOH	NaOAc	30
2	24	EtOH	NaOAc	68
3	24	Dry EtOH	NaOAc	65
4	24	MeOH	K_2CO_3	60
5	24	Dry MeOH	K_2CO_3	65

To keep pace with research needs, the condensation to make the 2,4-di-*iso*-propyl-6-pyridin-2-yl-1,2,4,5-tetrazinan-3-one (pyr-tetrazane) was gradually scaled up to a 5-gram quantity. While the yields remained relatively constant during the scale-up process, a new problem was encountered with the 5-gram scale reactions. After concentrating to a crude solid, the material appeared hygroscopic and had poor solubility in organic solvents with partial solubility in water. Samples taken for ^{1}H NMR and presented in Figure II.2 revealed a broad singlet at 4.25 ppm while two of the peaks had a different chemical shift compared to the literature.[13] An aqueous workup was performed on the sample and resulted in the spectrum labeled After Aqueous Workup in Figure II.2. Given that the aqueous workup removed the broad singlet and resulted in the correct chemical shifts of the two highlighted peaks, it is possible that the pyr-tetrazane was simply protonated. If it was an impurity, it is unlikely that it would reverse the chemical shifts of the peaks labeled A and B. This problem occurred for both sodium acetate and potassium carbonate reactions, but only on the 5-gram scale reactions. Consequently, the aqueous workup gave high purity product and did not require recrystallization.

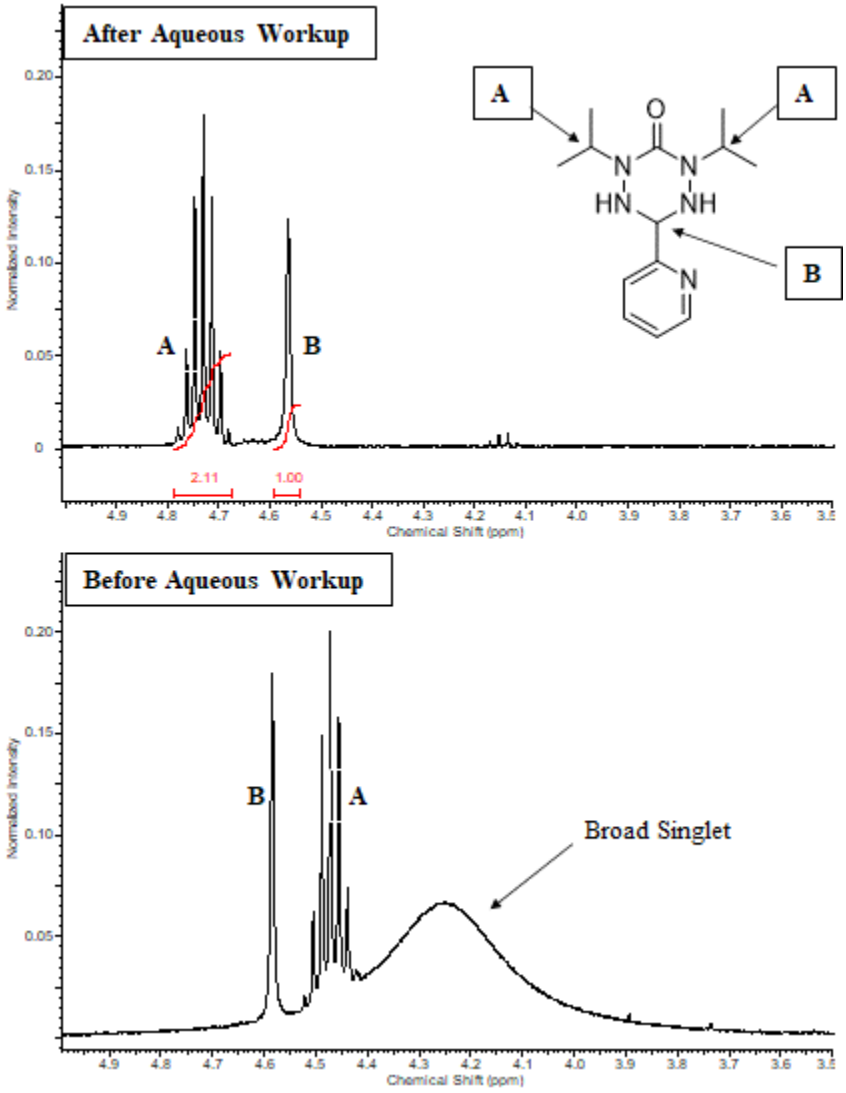

Figure II.2: ^{1}H NMR comparison for large scale condensation reaction. Both samples were run in DMSO-d_6.

The final reaction for the verdazyl ligand is the oxidation of the pyr-tetrazane to 1,5-di-*iso*-propyl-3-pyridin-2-yl-6-oxoverdazyl (VDZ), as shown in Scheme II.3. Following literature[13] precedent, the pyr-tetrazane and *p*-benzoquinone were dissolved in toluene and refluxed for 2 hours. Upon completion, the hydroquinone precipitate was filtered out and the filtrate was concentrated before using column chromatography to afford the red-green VDZ crystals. Attempts to increase the yield by varying the time at reflux gave minimal results as shown in

Table II.3. The two-hour mark was determined to be the optimal time while any longer is potentially harmful.

Table II.3: Oxidation yields for varying reaction times.

Entry	Time (hrs)	Solvent	Yield (%)
1	1	Toluene	41
2	2	Toluene	53
3	3	Toluene	50
4	4	Toluene	47

Upon Successful oxidation, the verdazyl ligand synthesis is complete. Commercially available starting materials combined with simple and high yielding reactions make the synthesis of this particular oxoverdazyl very favorable. Scale up attempts generally gave straightforward results except for the condensation to form pyr-tetrazane. However, a small adaptation to the procedure solved the problems, making the reaction scalable. These characteristics made the verdazyl ligand synthesis straightforward and optimizable.

II.3 Platinum Complex Synthesis

II.3.A Retrosynthetic Look at VDZ-Pt-CAT

The targeted complex shown in Figure II.3 is a novel compound and consists of two isomers. At the time of writing, there are no published synthetic routes involving the 1,5-di-*iso*-propyl-3-pyridin-2-yl-6-oxoverdazyl (VDZ) and platinum(II) metal center with the catecholate ligand. Figure II.3 contains both stereoisomers of the [3,5-di-*tert*-butylcatecholato(1,5-diisopropyl-3-pyridin-2-yl-6-oxoverdazyl)]platinum(II) (VDZ-Pt-CAT) complex.

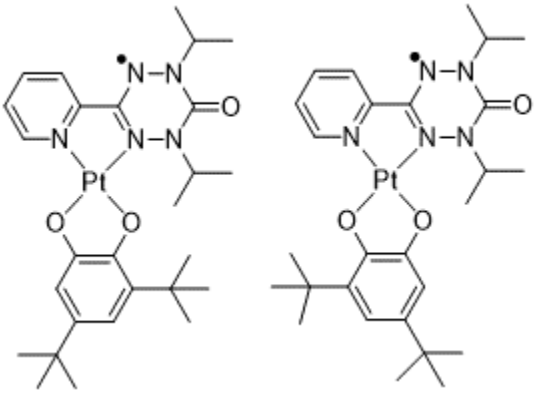

Figure II.3: Isomers of VDZ-Pt-CAT

There are two ways to approach the synthesis of VDZ-Pt-CAT which are shown in Scheme II.4. The key difference being the order of ligand coordination. Both routes **A** and **B**

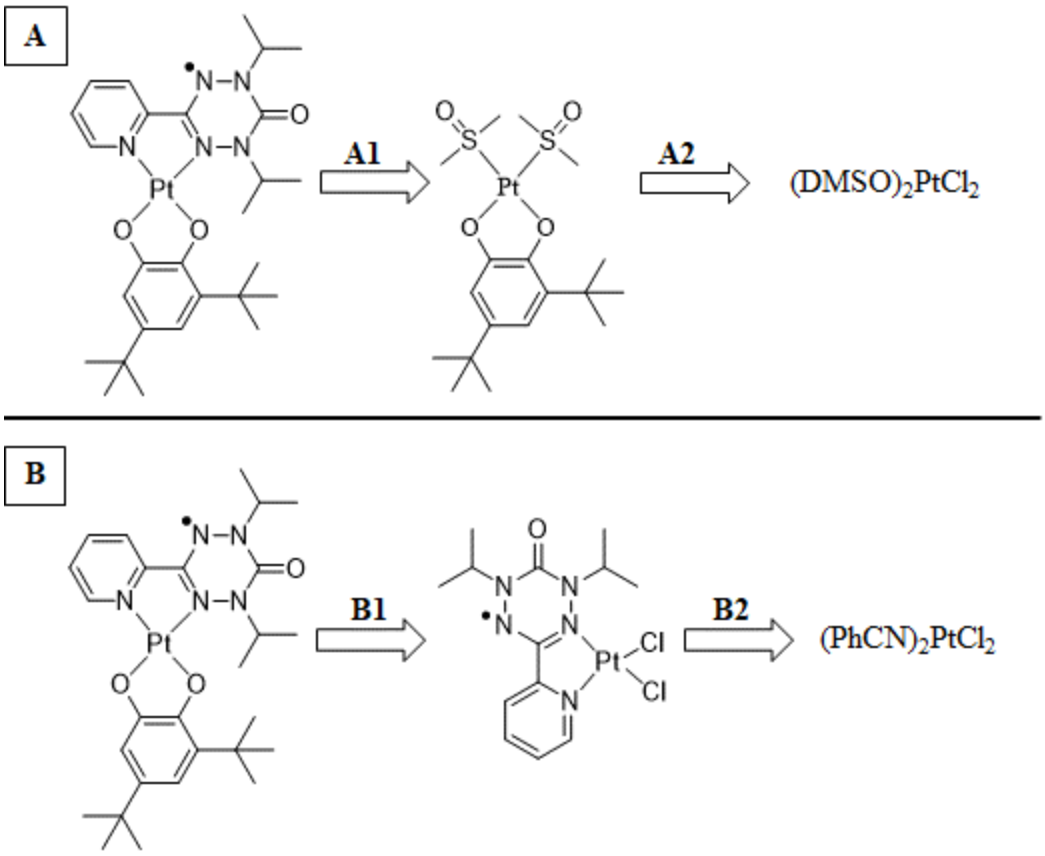

Scheme II.4: Two paths to VDZ-Pt-CAT.

have literature precedents for the **A2** and **B2** steps. The true novelty will be **A1** and **B1**. Due to synthetic challenges, both paths were explored in detail.

II.3.B The VDZ-based Approach

With both approaches equal in terms of existing research, the VDZ-based approach was chosen for the simplicity of the initial reactions and the expectation that chlorides would be favorable for ligand substitution. Scheme II.5 contains the synthesis of VDZ-$PtCl_2$, all of which is available in the literature.[9]

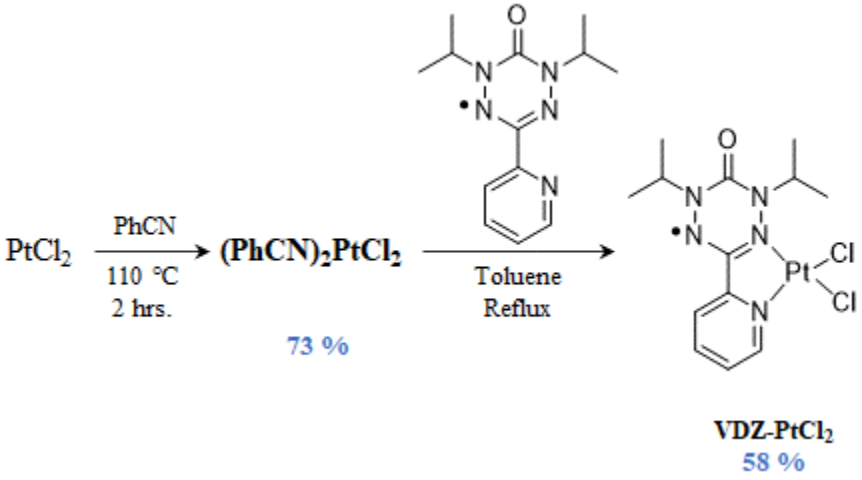

Scheme II.5: Synthesis of the VDZ-$PtCl_2$

Synthesis of the bis(benzonitrile)dichloroplatinum(II) complex ($(PhCN)_2PtCl_2$) is straightforward and results in good yields. The commercially available $PtCl_2$ was dissolved in a large excess of benzonitrile and heated to 110 ℃ for 2 hours. Upon cooling, hexane was used to initiate precipitation and the product was then collected. Further purification was unnecessary and the $(PhCN)_2PtCl_2$ was used as collected for the next reaction.

To begin the coordination of the VDZ ligand, $(PhCN)_2PtCl_2$ was dissolved in toluene. The platinum chloride salt is not readily soluble in toluene and had to be stirred or gently heated to be thoroughly dissolved before heating to reflux. After reflux, the reaction was left to cool

Table II.4: VDZ-$PtCl_2$ reflux time and associated yields.

Entry	Reflux Time (hrs)	Solvent	Yield (%)
1	0.5	Toluene	39
2	1	Toluene	44
3	2	Toluene	49
4	3	Toluene	58
5	4	Toluene	40

overnight. During this time, the VDZ-$PtCl_2$ precipitated and was collected and washed with toluene. Following the literature[9] procedure gave a 39 % yield and represents the first entry in Table II.4. A gradual increase in reflux time was observed to increase the yield, up to a point. The product will start precipitating during reflux which results in charred and unusable material. Therefore, refluxing longer than 3 hours was found to be more harmful than helpful.

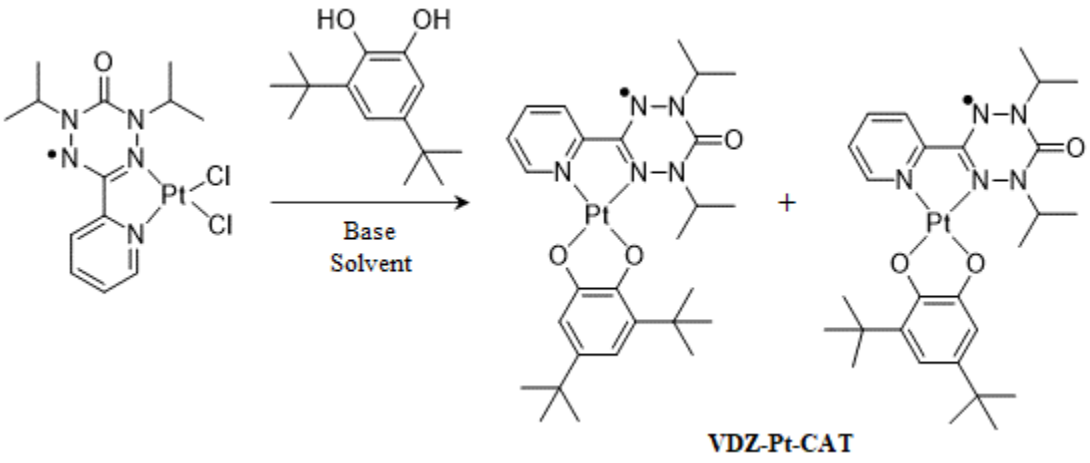

Scheme II.6: Generic Reaction Scheme for VDZ-Pt-CAT from VDZ-$PtCl_2$.

With VDZ-$PtCl_2$ in hand, the VDZ-Pt-CAT reaction was undertaken using literature conditions that use a bipyridine ligand to make a (bpy)Pt-CAT type complex.[15] A generic reaction scheme for the complexation is shown in Scheme II.6. These conditions included using deoxygenated DMSO as the solvent and potassium carbonate as the base and can be seen in Table II.5 as entry number one. However, these conditions resulted in decomposition. Decomposition in this case means the reaction mixture contained a significant amount of the uncoordinated VDZ ligand and no noticeable amounts of starting material or product. The only easily identifiable decomposition product for this reaction was the VDZ ligand due to its easily recognizable ^{14}N-hyperfine pattern and UV/Vis band. Following the decomposition result, it was determined that VDZ-$PtCl_2$ decomposes in the presence of DMSO. With this knowledge, the

Table II.5: Reaction Conditions

Entry	Solvent	Base	Temp. (°C)	Time (hrs)	Result	Reaction Type
1	DMSO	K_2CO_3	25	15	Decomposition	-
2	DMSO	K_2CO_3	50	15	Decomposition	-
3	THF/MeOH	KOH	25	2	Decomposition	Sequential
4	THF/MeOH	KOH	25	24	Decomposition	Sequential
5	THF/MeOH	KOH	50	2	Decomposition	Sequential
6	THF/MeOH	KOH	50	24	Decomposition	Sequential
7	THF/MeOH	KOH	25	2	Decomposition	Non-Sequential
8	THF/MeOH	KOH	25	24	Decomposition	Non-Sequential
9	THF/MeOH	KOH	50	2	Decomposition	Non-Sequential
10	THF/MeOH	KOH	50	24	Decomposition	Non-Sequential

reaction conditions were changed to those used by a collaborator of the Shultz Group, the Kirk Group, for a similar VDZ Pt(II) complex which has yet to be published. These conditions involved the use of freshly distilled THF and minimal, deoxygenated methanol with potassium hydroxide as the base. Yet, these conditions gave the same result: decomposition via

displacement of the VDZ ligand. As was done previously, solvents were tested and results are listed in Table II.6. It was determined that methanol can cause decomposition when present in large excess, but freshly distilled THF caused no decomposition. To reproduce reaction conditions as accurately as possible, the minimal amount of deoxygenated methanol needed to dissolve the base was measured and that amount was added to a solution of freshly distilled THF

Table II.6: Solvent List for VDZ-$PtCl_2$

Entry	Solvent	Result	Solubility
1	MeOH	Decomposition	Good
2	DCM	Decomposition	Good
3	DMSO	Decomposition	Good
4	THF	Safe	Good
5	Ether	Safe	Poor
6	Hexanes	-	Insoluble
7	MeCN	Safe	Good
8	Toluene	-	Insoluble

and VDZ-$PtCl_2$. It amounted to approximately 8 % by volume of the total solvent volume. In these conditions, the VDZ-$PtCl_2$ had minimal decomposition. Following these same steps, the base was added to the procedure and resulted in swift decomposition. With observations showing that the starting materials were susceptible to base, the reaction procedure was altered slightly. Table II.5 has a column that lists most of the entries as sequential and non-sequential. Non-sequential reactions were cases in which the VDZ-$PtCl_2$, catechol and base were all added to a reaction vessel and the system was purged before adding the solvent. These were the initial reaction conditions. With the base sensitivity issue identified and the solvent problem solved, the conditions were changed to sequential. This means a catecholate solution of base and minimal solvent were made and then added to the existing solution of VDZ-$PtCl_2$ in freshly distilled THF,

all of which were under argon. The desire was to allow the base to deprotonate the catechol first and limit the starting material and base interactions. However, these conditions did not change the outcome. To check that this observed decomposition was truly stopping the reaction, the reactions were set up and run for 24 hours, but the reactions still failed. Attempts at heating were used in hopes that the VDZ ligand might re-coordinate but were unsuccessful.

Table II.7: Tested Bases

Entry	Solvent	Base	Result
1	THF/MeOH	KOH	Decomposition
2	THF	Et_3N	Safe
3	THF	butylamine	Decomposition
4	THF	*tert*-butylamine	Decomposition

The VDZ-$PtCl_2$ was subjected to amine bases in anticipation that the amine bases would be milder and therefore less destructive. Three amine bases were tested and are shown in Table II.7 before deciding on triethylamine. Freshly distilled triethylamine had minimal effect on the starting material in THF. With a suitable amine base found, reactions were conducted following a non-sequential method. Triethylamine does not fully deprotonate the catechol and the VDZ-$PtCl_2$ has sufficient stability to withstand the temporary presence of triethylamine. Therefore, sequential methods were unnecessary to minimize base and starting material interactions. The VDZ-$PtCl_2$ and catechol were added to a Schlenk flask and purged, refilling with argon. Freshly distilled THF was then added, and the reaction allowed to stir for approximately 30 minutes. This initial stirring was implemented in anticipation that the catechol might engage in some form of coordination with the platinum center prior to the addition of base. After stirring, freshly distilled triethylamine was added to the reaction and the solution heated to reflux. Different reaction conditions were tested and are presented in Table II.8. The reaction solution was then

concentrated to dryness, taken into minimal toluene and loaded onto silica gel. The product was then eluted with 55 % ether in hexanes to afford the highly desired, dark purple VDZ-Pt-CAT.

Reaction conditions using 1 equivalent of catechol at room temperature for varying times, as shown in Table II.8. These conditions were then tested at reflux. Both resulted in no noticeable product formation with the presence of starting materials. The equivalents of catechol were then increased to 1.5 and gave no yields at room temperature. However, 1.5 equivalents at reflux for any time over 1 hour gave noticeable amounts of product. Purification attempts

Table II.8: Reaction conditions for VDZ-Pt-CAT.

Entry	Solvent	Base	CAT Equiv.	Time (hrs)	Temp. (°C)	Yield (%)
1	THF	Et_3N	1	0.5	25	No Rxn
2	THF	Et_3N	1	1	25	No Rxn
3	THF	Et_3N	1	2	25	No Rxn
4	THF	Et_3N	1	3	25	No Rxn
5	THF	Et_3N	1	0.5	66	No Rxn
6	THF	Et_3N	1	1	66	No Rxn
7	THF	Et_3N	1	2	66	No Rxn
8	THF	Et_3N	1	3	66	No Rxn
9	THF	Et_3N	1.5	0.5	25	No Rxn
10	THF	Et_3N	1.5	3	25	No Rxn
11	THF	Et_3N	1.5	0.5	66	No Rxn
12	THF	Et_3N	1.5	1	66	< 4
13	THF	Et_3N	1.5	2	66	< 4
14	THF	Et_3N	1.5	3	66	< 4
15	THF	Et_3N	2	1	66	5
16	THF	Et_3N	2	2	66	7
17	THF	Et_3N	2	3	66	10
18	THF	Et_3N	2.5	1	66	12
19	THF	Et_3N	2.5	2	66	15
20	THF	Et_3N	2.5	3	66	17

resulted in mostly residue of the desired product which was only enough for analysis by EPR. The number of equivalents of catechol were once again increased to 2.0 and reactions were run only at reflux. These changes resulted in consistent yields (~10%) that gave isolatable amounts of solid material. Increasing the catechol equivalents to 2.5 gave another increase in yields that varied by the amount of time at reflux. However, at 2.5 equivalents of catechol, new impurities were emerging and complicating purification. Further increasing the amount of catechol could present greater yields, but the primary impurity appearing with the increasing amounts of catechol is very difficult to remove from VDZ-Pt-CAT with column chromatography.

Column chromatography conditions were a challenge to determine due to the limited range of solvents possible. Like the VDZ-$PtCl_2$, the VDZ-Pt-CAT was unstable in several solvents. Significant amounts of product were lost due to unsuitable chromatography conditions for VDZ-Pt-CAT. After many trials and errors, it was found that concentrating the crude reaction mixture to dryness and taking it into minimal toluene to load on the silica gel column assembled with 55 % ether in hexanes gave the best results. Recall from Table II.6 that VDZ-$PtCl_2$ is insoluble in toluene. By loading the product with toluene, the remaining VDZ-$PtCl_2$ could be removed and not loaded on the column. Plus, the catechol impurities are pulled down the column with the toluene as it is flushed out. While VDZ-Pt-CAT has poor solubility in ether and hexanes, these solvents provide the best outcomes. But the most important issue regarding purification, handling and storage of the VDZ-Pt-CAT is that it cannot stay in solution for extended periods! Regardless of the solvent, leaving VDZ-Pt-CAT in solution can result in decomposition via displacement of the VDZ ligand. This makes prompt purification and dry storage imperative for VDZ-Pt-CAT.

With the synthesis of the VDZ-Pt-CAT completed, this method could be considered successful, though low-yielding. The primary difficulties faced in this synthetic approach were the reagent and product sensitivities to certain bases and solvents. Upon observing decomposition with KOH, the base was switched to an amine base in effort to avoid the hydroxide anion as it was believed this could be displacing the VDZ ligand due to its nucleophilicity. An interesting observation from switching to the amine bases was that the decomposition experienced with butylamine and *tert*-butylamine wasn't just VDZ ligand displacement, but also VDZ ligand decomposition. EPR data revealed a change in the nine-line pattern characteristic of the oxoverdazyl, suggesting an interaction between the base and VDZ. However, this was not explored as triethylamine was found to be suitable. Triethylamine was the bulkiest base attempted and gave the best results. With a suitable base, a suitable solvent was needed. The best results were achieved with THF. Though some solvents cause more immediate decomposition, all solvents tested had the potential to cause decomposition given enough time. Given the stability of the uncoordinated VDZ ligand and the observations concerning bases and solvents, it is believed that the coordinated VDZ will undergo substitution or displacement if conditions provide a potential pathway.

II.3.C The Catecholate-based Approach

The catecholate-based approach was chosen due to difficulties with the VDZ-based approach as well as expectations that dealing with the catechol reaction byproducts before VDZ coordination could remove potential interference from byproducts. The VDZ-based approach had significant hurdles due to the instability of the VDZ-$PtCl_2$ in certain solvents and bases so the catecholate-based approach was contrived to keep the coordination of the VDZ ligand as the

final step. This would eliminate the use of bases in the presence of a coordinated VDZ ligand and rely on ligand substitution of an easily replaced precursor ligand.

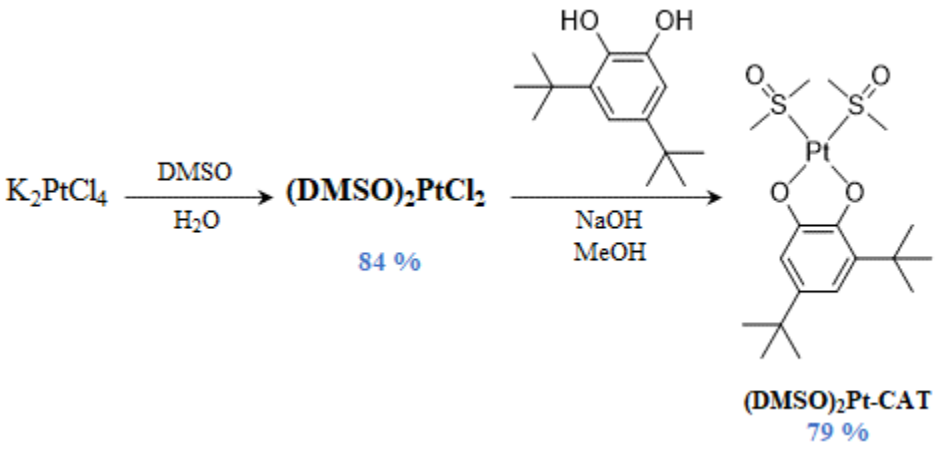

Scheme II.7: Synthetic scheme for making the $(DMSO)_2Pt$-CAT precursor complex.

The initial steps of this approach are present in the literature and shown in Scheme II.7. Starting with potassium tetrachloroplatinate(II) dissolved in minimal water, DMSO is added and the reaction is left stirring overnight. The precipitate was then collected and washed with ethanol and ether to yield the $(DMSO)_2PtCl_2$ in good yields. Following the synthesis of the dichloride, the $(DMSO)_2Pt$-CAT was synthesized according to the literature[16]. While maintaining an inert

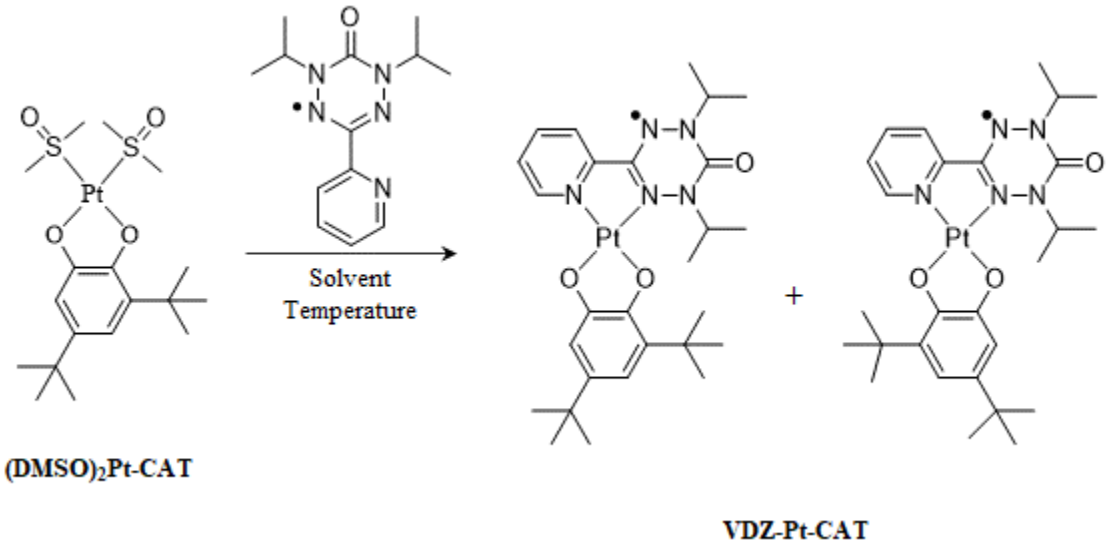

Scheme II.8: General scheme for the catecholate-based synthesis of VDZ-Pt-CAT.

atmosphere, NaOH and 3,5-di-*tert*-butylcatechol were dissolved in deoxygenated methanol. This

Table II.9: Reaction conditions using toluene or xylene.

Entry	Solvent	SM:VDZ Equiv.	Time (hrs)	Temp. (°C)	Result
1	Toluene	1 : 1	1	25	No Rxn
2	Toluene	1 : 1	2	25	No Rxn
3	Toluene	1 : 1	3	25	No Rxn
4	Toluene	1 : 1	15	25	No Rxn
5	Toluene	1 : 1	15	50	No Rxn
6	Toluene	1 : 1	1	110	No Rxn
7	Toluene	1 : 1	2	110	No Rxn
8	Toluene	1 : 1	3	110	No Rxn
9	Toluene	1 : 1	15	110	Decomposition
10	Toluene	1 : 2.2	1	25	No Rxn
11	Toluene	1 : 2.2	2	25	No Rxn
12	Toluene	1 : 2.2	3	25	No Rxn
13	Toluene	1 : 2.2	15	25	No Rxn
14	Toluene	1 : 2.2	15	50	No Rxn
15	Toluene	1 : 2.2	1	110	No Rxn
16	Toluene	1 : 2.2	2	110	No Rxn
17	Toluene	1 : 2.2	3	110	No Rxn
18	Toluene	1 : 2.2	15	110	Decomposition
19	Xylene	1 : 1	2	25	No Rxn
20	Xylene	1 : 1	15	25	No Rxn
21	Xylene	1 : 1	2	50	No Rxn
22	Xylene	1 : 1	1	120	No Rxn
23	Xylene	1 : 1	2	120	No Rxn
24	Xylene	1 : 1	3	120	Decomposition
25	Xylene	1 : 2.2	2	25	No Rxn
26	Xylene	1 : 2.2	15	25	No Rxn
27	Xylene	1 : 2.2	2	50	No Rxn
28	Xylene	1 : 2.2	1	120	No Rxn
29	Xylene	1 : 2.2	2	120	No Rxn
30	Xylene	1 : 2.2	3	120	Decomposition

solution was then added to a flask containing $(DMSO)_2PtCl_2$ and left stirring overnight. Upon completion, column chromatography afforded the desired $(DMSO)_2$Pt-CAT complex in good yields.

The final step in the synthesis involves replacing the two DMSO ligands with the bidentate VDZ ligand and follows the general scheme in Scheme II.8. Initial conditions include the use of toluene and are shown in Table II.9. With reagent equivalents held constant, varying the temperature from room temperature to reflux had no effect except for decomposition for the 15-hour reflux entry. The equivalents were then changed to include an excess of VDZ and the same reaction conditions were repeated. Still, no observable amounts of product were formed. The solvent was then changed to xylene and the same conditions were repeated, but with fewer

Table II.10: Other solvent combinations.

Entry	Solvent	SM:VDZ Equiv.	Time (hrs)	Temp. (°C)	Result
1	THF : Toluene	1 : 2.2	2	25	No Rxn
2	THF : Toluene	1 : 2.2	15	25	No Rxn
3	THF : Toluene	1 : 2.2	2	66	No Rxn
4	THF : Toluene	1 : 2.2	15	66	No Rxn
5	$CHCl_3$: Toluene	1 : 2.2	2	25	No Rxn
6	$CHCl_3$: Toluene	1 : 2.2	15	25	No Rxn
7	$CHCl_3$: Toluene	1 : 2.2	2	61	No Rxn
8	$CHCl_3$: Toluene	1 : 2.2	15	61	No Rxn
9	H_2O : Toluene	1 : 2.2	2	25	No Rxn
10	H_2O : Toluene	1 : 2.2	15	25	No Rxn
11	H_2O : Toluene	1 : 2.2	2	100	No Rxn
12	H_2O : Toluene	1 : 2.2	15	100	No Rxn
13	MeCN	1 : 2.2	15	25	No Rxn
14	MeCN	1 : 2.2	15	50	No Rxn
15	MeCN	1 : 2.2	15	75	No Rxn

room temperature attempts. By changing to xylene, the polarity would stay relatively unchanged, but the temperature of the reaction could be increased. The intent was to observe the effect of temperature without changing to more polar solvents. Temperatures could be increased to 120 ℃ for up to 3 hours before decomposition was observed. The decomposition for these reactions comprises the breakdown of the $(DMSO)_2$Pt-CAT into colloidal platinum and other unidentifiable products. The VDZ was still intact in almost all reaction attempts. With an increase in temperature yielding no results, other solvent combinations were attempted and are shown in Table II.10. Mixtures of THF and toluene or chloroform and toluene were used to gently adjust the polarity but yielded no results. The mixture of water and toluene was used with the aim of pulling the DMSO into the aqueous layer while keeping the VDZ, which has poor solubility in water, in the organic layer. Again, all attempts with these solvents failed. Finally, acetonitrile was utilized due to its greater polarity, but no reaction or decomposition were

Table II.11: Benzonitrile conditions.

Entry	Solvent	SM:VDZ Equiv.	Time (hrs)	Temp. (℃)	Result
1	Benzonitrile	1 : 1	2	25	No Rxn
2	Benzonitrile	1 : 1	15	25	No Rxn
3	Benzonitrile	1 : 1	2	50	No Rxn
4	Benzonitrile	1 : 1	15	50	No Rxn
5	Benzonitrile	1 : 1	1	110	5%
6	Benzonitrile	1 : 1	2	110	6%
7	Benzonitrile	1 : 1	3	110	Decomposition

observed.

Following the failure of adjustments to polarity and temperature individually, benzonitrile was chosen both for its polarity and high boiling point. In maintaining consistency with previous attempts, room temperature and mild heating were tried with varying reaction

times and are shown in Table II.11. With no product formation observed, the temperature was increased to 110 ℃ for 1 hour and resulted in a 5 % yield. Increasing the time to 2 hours gave no increase in yield and 3 hours resulted in decomposition.

With low yielding, but reproducible reaction conditions found, the next challenge was purification. As opposed to the VDZ-based approach, this reaction contained significant impurities. Instead of just starting materials, the crude reaction mixture contained uncoordinated VDZ, product, colloidal platinum and many other unidentifiable impurities. Purifying this viscous sludge required 5 % MeCN in toluene with a 300:1 ratio of silica gel to starting material. This is often followed up by a second column with similar conditions to remove impurities that couldn't be separated with the first column. If the product survives two columns, one is greeted with an abysmal 5-7 % yield of a dark colored solid. Recall from the VDZ-based approach that the product was purple in color, which is different when compared to this result. This question can only be answered by characterizing both results. The characterization is discussed in Chapter III in detail.

Though lacking elegance, the catecholate-based approach yielded results. With no base to account for, reaction conditions came down to finding compatible solvents and the subsequent time and temperature needed. The VDZ-based approach gave decomposition in the form of ligand displacement and was much easier to monitor through EPR. This approach, however, had no suitable means for monitoring the reaction in detail. Successful reaction conditions gave catastrophic decomposition of the $(DMSO)_2$Pt-CAT starting material. Microwave reactions were also attempted in efforts to provide energy without the increase in temperature but gave even worse results. With such unfavorable conditions, this approach was deemed less desirable than the VDZ-based approach.

II.3.D Conclusions Regarding the Synthetic Approaches

While both synthetic approaches yielded successful conditions, the VDZ-based approach gave clearly superior results. Ligand exchange at d^8 center square planar Pt(II) complexes has been researched and shown to undergo an associative mechanism in most situations.[17–19] This associative mechanism signifies the formation of a five-coordinate intermediate with the incoming ligand. For the VDZ-based approach, that would mean the 3,5-di-*tert*-butylcatechol. The pK_{a1} of catechols is approximately 8.9 and the pK_{a2} is roughly 13.9.[20] The pK_a of the conjugate acid of triethylamine is about 10.7 according to Evans pK_a Table. Triethylamine can deprotonate the first OH but not the second, at least while uncoordinated. However, looking at Table II.8, it required at least 1.5 equivalents of catechol before product was even noticeable by EPR or TLC. Increasing the number of equivalents of catechol gave increased yields. It is possible that the increased concentration of catechol showed effect, but it could also be that the catechol acted as the base. The triethylamine will deprotonate the first OH either before or after coordination. However, once the five-coordinate intermediate forms, the area around the second OH becomes more hindered due to sterics of both the VDZ and catechol *tert*-butyl groups. Setting pKa aside, it is entirely possible that the remaining triethylamine simply cannot reach the other OH. The catechol certainly contains steric bulk as well, but if the triethylamine deprotonates the first OH of the catechol, it is possible that the catechol has an easier fit to access the other OH of the intermediate due to it having a more structured skeleton. But increasing the catechol was also accompanied by increasing the equivalents of triethylamine at the same rate. To ensure that a simple excess of triethylamine wasn't the answer, test reactions with 1.5 equivalents of catechol and 3.5 equivalents of base were attempted. Excess base gave no favorable conditions.

For the catecholate-based approach, conclusions are difficult to draw concerning the possible mechanism. The reaction results in catastrophic decomposition of starting material with poor yields. The $(DMSO)_2$Pt-CAT is essentially torn apart as product forms. The conclusion that can be drawn is that the reaction needs high temperature, not just polar solvents or energy via microwave. Recall that the VDZ-$PtCl_2$ also needed high temperature and the ligands that were being displaced were benzonitriles. In this case, high temperature and benzonitrile were also needed. Going along with this line of thought, $(PhCN)_2$Pt-CAT was attempted but the attempts resulted in failure to coordinate the benzonitrile as ligands. Unlike the VDZ-based approach where starting materials remain with the triethylamine attempts, everything but VDZ is destroyed with this approach which makes it impossible to track the starting materials. Notably, though, is that this approach has no issues with reproducibility despite the decomposition issues. Whatever the exact mechanism is, it delivers consistent results.

II.4 VDZ-Pt-SQ

With the synthetic route of the title complex secured, the final step for this research project involved the oxidation of the VDZ-Pt-CAT to VDZ-Pt-SQ. Generating this new biradical would allow further study of the electronic structure. Like the monoradical, the biradical was also an unknown compound at the time of writing. Compared to the synthetic struggles of the VDZ-Pt-CAT, the oxidation was performed with relative ease and the conditions are shown in Scheme II.9. Under inert atmosphere, the VDZ-Pt-CAT was dissolved in minimal deoxygenated acetonitrile and 1.1 equivalents of a solution of oxidant in deoxygenated acetonitrile was added and the reaction stirred for 10-15 minutes. Methyl THF was then added and an aliquot was taken for EPR experiments. Both oxidants are partially soluble in THF and methyl THF which aided in the EPR experiments. The problems for this reaction were the limited tools at our disposal for

characterization. Purification has not proven helpful due to the unstable nature of the complex as aerobic conditions can result in decomposition and certain solvents can also cause decomposition. Choosing two different oxidizers and comparing the results was one method to help with this problem as the results should match. As anticipated, EPR data from both oxidations gave the same frozen solution EPR spectrum which is discussed in Chapter III. However, a previous oxidation using the same methodology and ferrocenium tetrafluoroborate gave a different EPR spectrum which is further discussed in Chapter III.

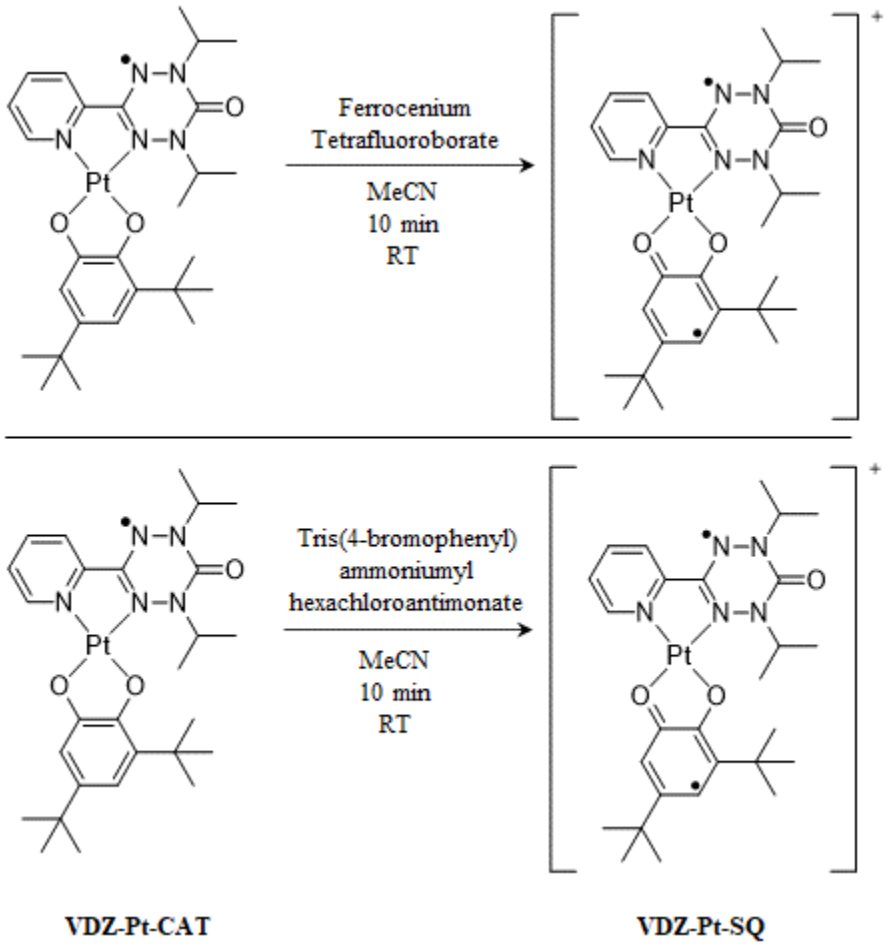

Scheme II.9: Oxidation of VDZ-Pt-CAT.

II.5 Experimental

General. Reagents and solvents were purchased from vendors and used as received unless otherwise noted. All EPR spectra were recorded on a Bruker ELEXSYS E500 cw X-band spectrometer. ^{1}H and ^{13}C NMR spectra were recorded on a Varian Mercury 400 MHz or a Bruker NEO 400 MHz spectrometer at room temperature. ^{1}H and ^{13}C chemical shifts are listed in parts per million (ppm) and are referenced to residual protons or carbons of the deuterated solvents, respectively. Mass Spectrometry data was collected by the METRIC labs at NC State University. UV/Vis spectra were collected on a UV-3600 Shimadzu UV-Vis-NIR spectrometer while UV/Vis spectroelectrochemical oxidation experiments were conducted in a glovebox using a Honeycomb Spectroelectrochemical Cell Kit. Spectroelectrochemical measurements were acquired with an Ocean Optics HR2000+ spectrometer with a 0.1 M solution of $TBAPF_6$ in spectrophotometric grade MeCN as the supporting electrolyte and the $Ag/AgNO_3$ redox couple as an internal reference.

***tert*-Butyl-2-isopropylhydrazonecarboxylate (Boc-hydrazone)**. Prepared according to literature procedure.[14] *tert*-Butyl carbazate (1.00 g, 0.0075 mol) and acetone (5.5 mL, 0.075 mol) were added to a 25 mL round-bottom flask and left stirring overnight. The reaction was then concentrated under reduced pressure to give the title compound (1.27 g, 97 %). Product can be recrystallized with THF/Hexanes if needed. ^{1}H NMR (400 MHz, DMSO-d_6) δ = 9.33 (m, 1 H), 1.93 - 1.75 (m, 6 H), 1.44 (s, 9 H) ppm. ^{13}C NMR (400 MHz, DMSO-d_6) δ = 152.9, 149.9, 80.8, 28.2, 25.4, 16.0 ppm. Data consistent with literature.[7,14]

***tert*-Butyl-2-isopropylhydrazinecarboxylate (*i*-Pr-hydrazine)**. Adapted from literature procedure.[8,13,14] *tert*-Butyl-2-isopropylhydrazonecarboxylate (7.00 g, 0.040 mol) and sodium cyanoborohydride (3.83 g, 0.060 mol) were dissolved in dry MeOH (70 mL) in inert conditions

and cooled to 0 ℃. A solution of glacial acetic acid (3.5 mL, 0.060 mol) in dry MeOH (30 mL) was added dropwise while maintaining 0℃. After the addition, the reaction was allowed to warm to room temperature overnight while stirring. The reaction was then quenched by stirring with 6 M NaOH (40 mL) for 30 minutes. DCM was then used for extraction followed by washing with brine and drying with $MgSO_4$. The solvent was then removed *in vacuo* to afford the title compound (5.86 g, 83 %). Purification is possible with sublimation or recrystallization with THF/Hexanes if needed. ^{1}H NMR (400 MHz, DMSO-d_6) δ = 8.27 (s, 1 H), 4.24 (s, 1 H), 2.87 (m, 1 H), 1.38 (s, 9 H), 0.90 (d, J = 6.3 Hz, 6 H) ppm. ^{13}C NMR (400 MHz, DMSO-d_6) δ = 80.3, 50.7, 28.3, 20.6 ppm. Data consistent with literature.[7,14]

Di-*tert*-butyl-2,2′-carbonylbis-(2-isopropylhydrazine-carboxylate) (Boc-bis(hydrazide)). Adapted from literature procedure.[14] Tert-butyl 2-isopropylhydrazinecarboxylate (3.00 g, 0.017 mol) was dissolved in dry toluene (45 mL) while under nitrogen. Freshly distilled triethylamine (2.4 mL, 0.017 mol) was added and the reaction was cooled to 0 ℃. A separate solution of triphosgene (0.865 g, 0.0029 mol) in dry toluene (20 mL) was made and cannula transferred to the reaction vessel while maintaining temperature and inert atmosphere. Upon completion of the transfer, the reaction was allowed to warm to room temperature overnight while stirring. The copious amounts of triethylamine hydrochloride precipitate was then filtered out, washed with warm toluene and discarded. The filtrate was then concentrated and washed with heptane to afford a colorless solid (2.56 g, 80 %). Recrystallization with heptane can be used for further purification if needed. ^{1}H NMR (400 MHz, DMSO-d_6) δ = 8.43 (s, 2 H), 4.02 (m, J = 6.5 Hz, 2 H), 1.40 (s, 18 H), 1.01 (d, 12 H) ppm. ^{13}C NMR (400 MHz, DMSO-d_6) δ = 162.8, 155.9, 81.1, 52.4, 28.1, 19.3 ppm. Data consistent with literature.[13,14]

2,4-Diisopropylcarbonhydrazide bis-hydrochloride (bis(hydrazide) salt). Prepared according to literature procedure.[14] Di-*tert*-butyl-2,2′-carbonylbis-(2-isopropylhydrazine-carboxylate) (2.50 g, 0.0066 mol) was added to a 100 mL round-bottom flask with EtOH (40 mL) and a 35 % HCl solution (20 mL). The reaction was heated to 50 ℃ for 30 minutes while mild effervescence was observed. The reaction was then allowed to cool overnight before being concentrated under reduced pressure to give quantitative yield. The product was used without further purification for the next reaction. Samples for analysis were further purified by recrystallization from propanol. ^{1}H NMR (400 MHz, $CDCl_3$) δ = 4.06 (m, *J* = 6.1 Hz, 2 H), 1.23 (d, *J* = 6.1 Hz, 12 H) ppm. MP: 188-189 ℃. Data consistent with literature.[13]

2,4-Diisopropyl-6-pyridin-2-yl-1,2,4,5-tetrazinan-3-one (pyr-tetrazane). Prepared according to literature procedure.[13] 2,4-Diisopropylcarbonhydrazide bis-hydrochloride (141 mg, 0.57 mmol) and 2-pyridinecarboxaldehyde (0.054 mL, 0.57 mmol) were dissolved in the minimal amount of EtOH. A solution of sodium acetate (93 mg, 1.14 mmol) in EtOH was made and added to the reaction. The reaction was left stirring overnight. Upon completion, the reaction was filtered and concentrated to give a yellow residue. The residue was then recrystallized from heptane to give the desired product as a yellow solid (102 mg, 68 %). ^{1}H NMR (400 MHz, DMSO-d_6) δ = 8.66 (ddd, *J* = 5.0, 2.0, 1.0 Hz, 1 H), 8.03 (td, *J* = 7.7, 1.6 Hz, 1 H), 7.72 (dt, *J* = 7.9, 1.0 Hz, 1 H), 7.60 (ddd, 1 H), 4.58 (m, *J* = 6.6, 13.3 Hz, 2 H), 4.47 (s, 1 H), 1.07 - 0.96 (m, 12 H) ppm. ^{13}C NMR (400 MHz, DMSO-d_6) δ = 154.5, 153.6, 149.5, 137.2, 124.1, 123.6, 71.3, 47.6, 19.4, 18.4 ppm. MP: 159-162 ℃. Data consistent with literature.[13]

1,5-diisopropyl-3-pyridin-2-yl-6-oxoverdazyl (**VDZ**). Adapted from literature procedure.[13] 2,4-Diisopropyl-6-pyridin-2-yl-1,2,4,5-tetrazinan-3-one (300 mg, 0.0011 mol) and p-benzoquinone (184 mg, 0.0017 mol) were dissolved in toluene (20 mL) in a 100 mL round-bottom flask. The

solution was then refluxed for 2 hours while monitoring with TLC and EPR. Upon completion, the reaction was cooled to room temperature and the hydroquinone precipitate was filtered out and discarded. The filtrate was then concentrated to a residue and then purified with column chromatography using silica gel and 20 % EtOAc/Hexanes to afford red-orange crystals (155 mg, 53 %). Further purification can be carried out using DCM/Heptane for recrystallization if needed. UV/Vis (THF) 410, 450 nm. HRMS m/z: $[M+H]^+$ Theoretical for $C_{13}H_{18}N_5O$ 261.15841 ; Experimental 261.15862. MP: 121-123 ℃. Data consistent with literature.[13]

Bis(benzonitrile)dichloroplatinum(II) ($(PhCN)_2PtCl_2$). Prepared according to literature.[21] Platinum(II) dichloride (0.200 g, 0.00075 mol) and benzonitrile (7.7 mL, 0.075 mol) were added to a 25 mL round-bottom flask and heated to 110 ℃ for 2 hours. After cooling, hexane was added to initiate precipitation. The precipitate was then collected with vacuum filtration and washed with hexane to afford a pale-yellow solid (258 mg, 73 %). ^{1}H NMR (400 MHz, $CDCl_3$) δ = 7.85 (d, 4 H), 7.74 (t, 2 H), 7.60 (t, 4 H) ppm. Data consistent with literature.[21]

***cis*-Dichlorobis(dimethyl sulfoxide)platinum(II) ($(DMSO)_2PtCl_2$)**. Prepared according to literature.[22] Potassium tetrachloroplatinate(II) (0.500 g, 0.0012 mol) and H_2O (1 mL) were added to a 10 mL round-bottom flask. Dimethyl sulfoxide (0.25 mL, 0.0036 mol) was then added and the reaction stirred overnight. The precipitate was then collected and washed with ethanol and ether to afford the desired product (0.426 mg, 84 %). ^{1}H NMR ($CDCl_3$) δ = 3.51 (t, J = 10.0 Hz, 6H). Data consistent with literature.[22]

3,5-di-*tert*-butylcatecholato(dimethyl sulfoxide)platinum(II) ($(DMSO)_2$Pt-CAT). Prepared according to literature.[16] 3,5-di-*tert*-butylcatechol (220 mg, 0.99 mmol) and $(DMSO)_2PtCl_2$ (200 mg, 0.47 mmol) were added to a 100 mL round-bottom flask and purge-pumped three times, filling with argon. A solution of NaOH (79 mg, 1.9 mmol) in deoxygenated MeOH (20 mL) was

added to the reaction vessel and stirred overnight. The reaction was then concentrated to a residue and purified on silica gel with 2 % MeOH/DCM to afford a yellow solid (213 mg, 79 %). ^{1}H NMR (400 MHz, $CDCl_3$) δ = 6.68 (d, *J* = 2.1 Hz, 1 H), 6.57 (d, *J* = 2.1 Hz, 1 H), 3.58 - 3.54 (m, 12 H), 1.42 (s, 9 H), 1.29 (s, 9 H) ppm. Data consistent with literature.[16]

[1,5-diisopropyl-3-pyridin-2-yl-6-oxoverdazyl]dichloroplatinum(II) (**VDZ-PtCl$_2$**). Adapted from literature procedure.[9] VDZ (50 mg, 0.19 mmol) and $(PhCN)_2PtCl_2$ (99 mg, 0.21 mmol) were added to a 25 mL round-bottom flask and dissolved in toluene (5 mL). The reaction was heated to reflux for 3 hours while under nitrogen. It was then allowed to cool to room temperature overnight. The precipitate was then collected with vacuum filtration and washed with toluene to give a dark purple solid (59 mg, 58 %). UV/Vis (THF) 462, 525, 627, 677 nm. HRMS m/z: $[M]^-$ Theoretical for $C_{13}H_{18}Cl_2N_5OPt$ 525.05416; Experimental 525.05451. Data consistent with literature.[9]

VDZ-Pt-CAT. VDZ-$PtCl_2$ (50 mg, 0.095 mmol) and 3,5-di-*tert*-butylcatechol (32 mg, 0.14 mmol) were added to a 25 mL Schlenk flask and the flask was purge-pumped three times, refilling with argon. Freshly distilled THF (10 mL) was added to the flask and the solution stirred for 30 minutes. Freshly distilled triethylamine (0.040 mL, 0.28 mmol) was then added and the reaction heated to reflux for 2 hours while maintaining inert atmosphere. The reaction was then concentrated to a residue and loaded on silica gel with toluene (less than 2 mL) and eluted with 55 % ether/hexanes to yield a dark purple solid (7 mg, 10 %). HRMS m/z: $[M]^-$ Theoretical for $C_{27}H_{38}N_5O_3Pt$ 675.26279; Experimental 675.26434.

II.6 References

(1) Kuhn, R. Trischmann, H. Conspicuously Stable N-Containing Radicals. *Angew. Chemie* **1963**, *75*, 294–295.

(2) Koivisto, B. D.; Hicks, R. G. The Magnetochemistry of Verdazyl Radical-Based Materials. *Coord. Chem. Rev.* **2005**, *249* (23), 2612–2630. https://doi.org/10.1016/j.ccr.2005.03.012.

(3) Lipunova, G. N.; Fedorchenko, T. G.; Tsmokalyuk, A. N.; Chupakhin, O. N. Advances in Verdazyl Chemistry. *Russ. Chem. Bull.* **2020**, *69* (7), 1203–1222. https://doi.org/10.1007/s11172-020-2892-6.

(4) Wang, C.; Lin, S. Y.; Shi, W.; Cheng, P.; Tang, J. Exploiting Verdazyl Radicals to Assemble 2p-3d-4f One-Dimensional Chains. *Dalt. Trans.* **2015**, *44* (12), 5364–5368. https://doi.org/10.1039/c4dt03354j.

(5) Wu, W.; Li, X. Le; Fan, X. H.; Yang, L. M. An Easy Route to N,N-Diarylhydrazines by Cu-Catalyzed Arylation of Pyridine-2-Carbaldehyde Hydrazones with Aryl Halides. *European J. Org. Chem.* **2013**, No. 5, 862–867. https://doi.org/10.1002/ejoc.201201445.

(6) Johnston, C. W.; McKinnon, S. D. J.; Patrick, B. O.; Hicks, R. G. The First "Kuhn Verdazyl" Ligand and Comparative Studies of Its PdCl2 Complex with Analogous 6-Oxoverdazyl Ligands. *Dalt. Trans.* **2013**, *42* (48), 16829–16836. https://doi.org/10.1039/c3dt52191e.

(7) Santos, M. S.; Nortcliffe, A.; Lewis, W.; Bradshaw, T. D.; Moody, C. J. Synthesis of Highly Substituted 1,2-Diazetidin-3-Ones, Small-Ring Scaffolds for Drug Discovery.

Chem. - A Eur. J. **2018**, *24* (33), 8325–8330. https://doi.org/10.1002/chem.201801309.

(8) Giordano, C.; Calabretta, R.; Gallina, C.; Consalvi, V.; Scandurra, R.; Chiaia Noya, F.; Franchini, C. Synthesis and Inhibiting Activities of 1-Peptidyl-2-Haloacetyl Hydrazines toward Cathepsin B and Calpains. *Eur. J. Med. Chem.* **1993**, *28* (4), 297–311. https://doi.org/10.1016/0223-5234(93)90147-7.

(9) McKinnon, S. D. J.; Gilroy, J. B.; McDonald, R.; Patrick, B. O.; Hicks, R. G. Magnetostructural Studies of Palladium(Ii) and Platinum(Ii) Complexes of Verdazyl Radicals. *J. Mater. Chem.* **2011**, *21* (5), 1523–1530. https://doi.org/10.1039/c0jm02560g.

(10) Price, J. H.; Williamson, A. N.; Schramm, R. F.; Wayland, B. B. Palladium(II) and Platinum(II) Alkyl Sulfoxide Complexes. Examples of Sulfur-Bonded, Mixed Sulfur- and Oxygen-Bonded, and Totally Oxygen-Bonded Complexes. *Inorg. Chem.* **1972**, *11* (6), 1280–1284. https://doi.org/10.1021/ic50112a025.

(11) Miyashiro, S.; Ishii, T.; Miura, Y.; Yoshioka, N. Synthesis and Magnetic Properties of Stable Radical Derivatives Carrying a Phenylacetylene Unit. *Molecules* **2018**, *23* (2), 1–11. https://doi.org/10.3390/molecules23020371.

(12) Vertesaljai, P.; Lebedyeva, I. O.; Oliferenko, A. A.; Qi, X.; Fu, J.; Ostrov, D. A.; Asiri, A. M.; Dennis Hall, C.; Katritzky, A. Mimicking a Proline Tripeptide with Pyrazolidines and a Cyclopentane Linker. *Tetrahedron Lett.* **2015**, *56* (48), 6653–6655. https://doi.org/10.1016/j.tetlet.2015.09.063.

(13) Paré, E. C.; Brook, D. J. R.; Brieger, A.; Badik, M.; Schinke, M. Synthesis of 1 , 5-Diisopropyl Substituted 6-Oxoverdazyls . *Org. Biomol. Chem.* **2005**, *3233* (3), 99–100.

(14) Kumar, V.; Shova, S.; Maurel, V.; Novitchi, G.; Train, C. Crystallographic Insights into the Synthesis and Magnetic Properties of Oxoverdazyl Radicals Functionalized by Benzoic Acid. *Eur. J. Inorg. Chem.* **2018**, *2018* (3), 517–524. https://doi.org/10.1002/ejic.201700950.

(15) Kirk, M. L.; Shultz, D. A.; Chen, J.; Hewitt, P.; Daley, D.; Paudel, S.; Van Der Est, A. Metal Ion Control of Photoinduced Electron Spin Polarization in Electronic Ground States. *J. Am. Chem. Soc.* **2021**, *143* (28), 10519–10523. https://doi.org/10.1021/jacs.1c04149.

(16) Lebedeva, M. A.; Chamberlain, T. W.; Scattergood, P. A.; Delor, M.; Sazanovich, I. V.; Davies, E. S.; Suyetin, M.; Besley, E.; Schröder, M.; Weinstein, J. A.; Khlobystov, A. N. Stabilising the Lowest Energy Charge-Separated State in a {metal Chromophore-Fullerene} Assembly: A Tuneable Panchromatic Absorbing Donor-Acceptor Triad. *Chem. Sci.* **2016**, *7* (9), 5908–5921. https://doi.org/10.1039/c5sc04271b.

(17) BASOLO, F. Substitution Reactions of Square Planar Complexes. In *Mechanisms of Inorganic Reactions*; American Chemical Society, 1965; pp 81–106. https://doi.org/10.1021/ba-1965-0049.ch004.

(18) Burgess, J. Inert Metal Complexes: Co-Ordination Number Four. In *Inorganic Reaction Mechanisms (London)*; 1972; pp 142–162. https://doi.org/10.1039/9781847556509-00142.

(19) Housecroft, C.; Sharpe, A. *Inorganic Chemistry*, 4th ed.; Pearson, 2012.

(20) Romero, R.; Salgado, P. R.; Soto, C.; Contreras, D.; Melin, V. An Experimental Validated Computational Method for PKa Determination of Substituted 1,2-Dihydroxybenzenes. *Front. Chem.* **2018**, *6* (JUL), 1–11. https://doi.org/10.3389/fchem.2018.00208.

(21) Roy, S. S.; Appleby, K. M.; Fear, E. J.; Duckett, S. B. SABRE-Relay: A Versatile Route to Hyperpolarization. *J. Phys. Chem. Lett.* **2018**, *9* (5), 1112–1117. https://doi.org/10.1021/acs.jpclett.7b03026.

(22) Dang, H. T.; Lee, H. W.; Lee, J.; Choo, H.; Hong, S. H.; Cheong, M.; Lee, H. Enhanced Catalytic Activity of (DMSO)2PtCl2 for the Methane Oxidation in the SO3-H2SO4 System. *ACS Catal.* **2018**, *8* (12), 11854–11862. https://doi.org/10.1021/acscatal.8b04101.

Chapter III: Characterization of VDZ-Pt-CAT

III.1 Electronic Absorption Spectroscopy Results

The VDZ and VDZ-$PtCl_2$ precursors have been previously characterized in the literature.[1] The VDZ ligand has absorption maxima near 25000 cm^{-1} ($\varepsilon \sim 1900\ M^{-1}\ cm^{-1}$) and 22000 cm^{-1} ($\varepsilon \sim 500\ M^{-1}\ cm^{-1}$) which is consistent with literature.[1] The VDZ-$PtCl_2$ complex has absorption maxima between 22000 cm^{-1} and 14000 cm^{-1}. The two bands seen in the uncoordinated VDZ can also be seen in the VDZ-$PtCl_2$ but red-shifted by approximately 2000-3000 cm^{-1} and with increased intensity. Furthermore, there are more transitions present near 15000 cm^{-1} that were absent in the free VDZ ligand. The bands near 19000 and 22000 cm^{-1} of the VDZ-$PtCl_2$ complex are the ligand-based transitions while the bands around 15000 cm^{-1} could be metal-to-ligand (Pt

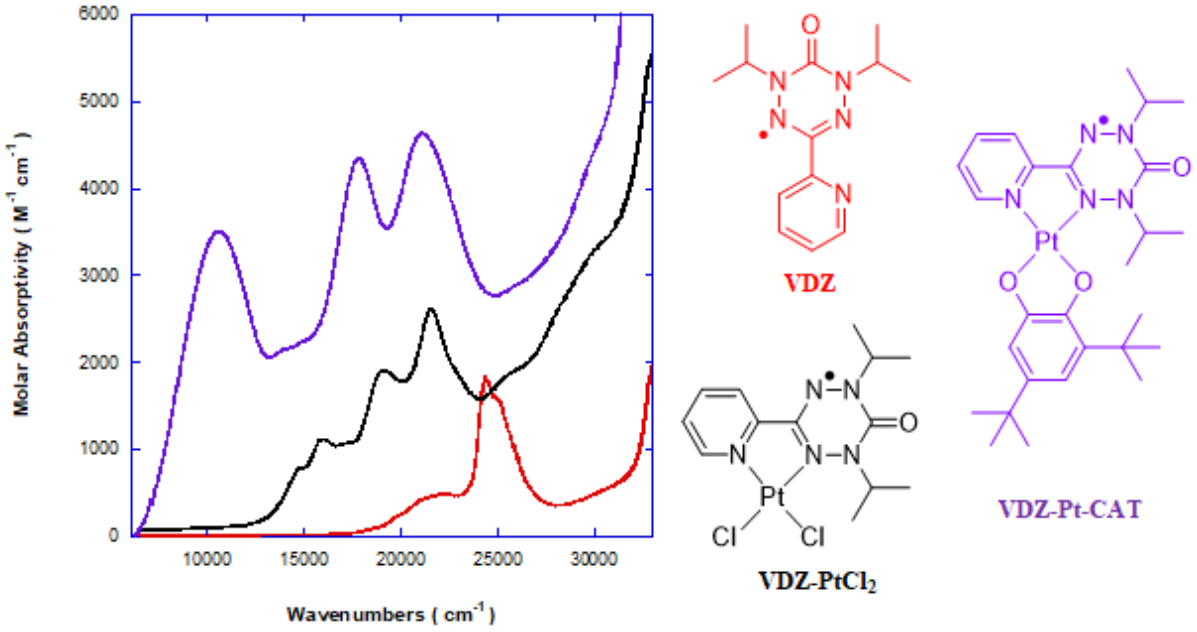

Figure III.1: Extinction coefficients of VDZ (red), VDZ-$PtCl_2$ (black) and VDZ-Pt-CAT (purple) in THF.

d-orbital) to VDZ π^* charge transfer (MLCT) bands given that the VDZ is a π-acceptor ligand

with a low-lying singly-occupied MO (SOMO). This assignment would be consistent with observations from literature regarding verdazyl-metal complexes.[1,2]

Looking at Figure III.1, one can see the significant changes in the spectrum with regards to the free VDZ and the platinum salt complex. The most obvious being the large feature near 10000 cm^{-1} ($\varepsilon \sim 3500\ M^{-1}\ cm^{-1}$) which is indicative of the coordinated catecholate. This intense feature is only present with the catecholate ligand and is likely the CAT → VDZ (SOMO) ligand-to-ligand charge transfer (LLCT). The two features near 17000 and 22000 cm^{-1} are likely the VDZ transitions mentioned previously but with a greater intensity. Those features around 15000 cm^{-1} found in the VDZ-$PtCl_2$ are not seen in the corresponding VDZ-Pt-CAT complex.

III.1.A Coordination Isomers

As mentioned in the synthetic discussion previously, there are two isomers possible for the desired VDZ-Pt-CAT complex: the more hindered and less hindered isomers. The hindered isomer is referring to possible steric interactions involving the *t*-butyl group of the CAT and the isopropyl group of the VDZ and can be seen in purple in Figure III.2. Mentioned previously was that the catechol-based approach gave a product with a color that was different from the VDZ-based approach which gave a purple-colored product. In addition to this, when purifying the crude reaction from the VDZ-based approach, a light gray band is sometimes isolated that gives the same EPR signal as the VDZ-Pt-CAT. This gray band is often isolated as nothing more than a residue and is therefore the minor product of the reaction. All data and observations indicate that these two different colored products are the two isomers.

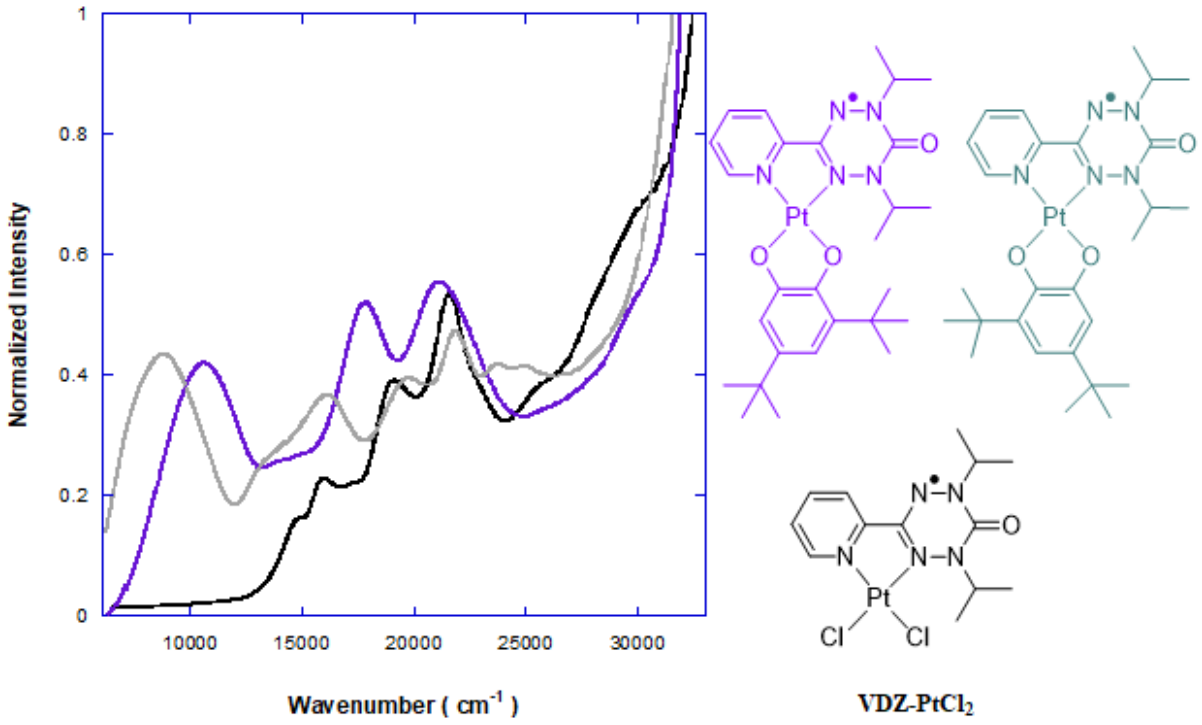

Figure III.2: UV/Vis data containing the VDZ-based approach product (purple) and the CAT-based approach (grey).

The purple product of the VDZ-based approach has been verified as the more hindered isomer. Shultz group collaborators at the University of New Mexico were able to grow crystals

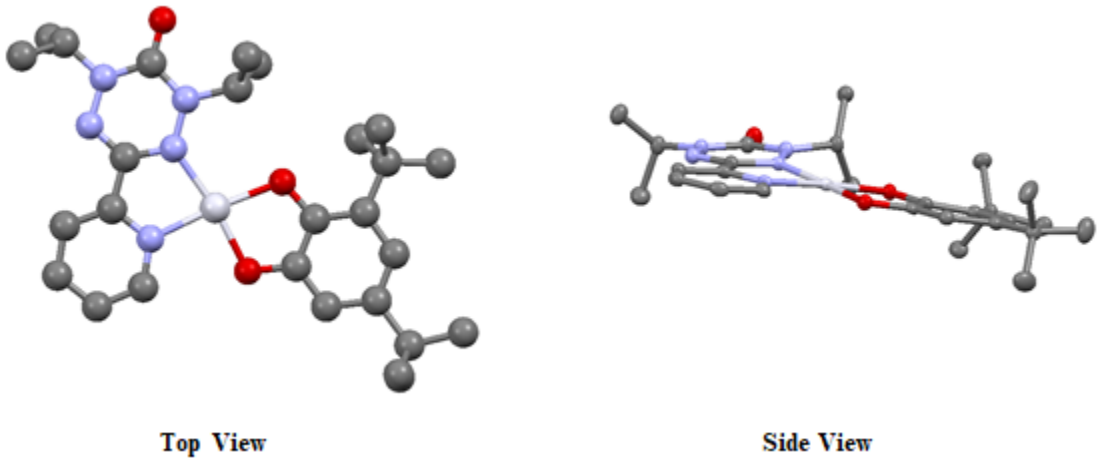

Figure III.3: X-ray structures of the purple-colored product (VDZ-Pt-CAT).

of this product and the results are shown in Figure III.3. The structures shown in Figure III.3 clearly indicate that the major product of the VDZ-based approach is the kinetic isomer. Given these observations, it is possible that the conjugate acid of the triethylamine is directing the formation of the kinetic isomer.

With the purple product being the more-hindered isomer, the thermodynamic isomer must be the other dark solid. In fact, mass spectrometry results prove that the other solid is also VDZ-Pt-CAT. Yet, one is purple, and the other is a dark solid that is gray/olive in solution in low concentrations. Figure III.2 shows that the dark solid has features similar to those found in the VDZ-$PtCl_2$ which is a dark purple/dark brown solid. The less hindered product displays the features from the VDZ-$PtCl_2$ that were not clearly displayed in the more hindered isomer. These transitions are presumed to be MLCT bands which would imply that something about the more hindered isomer obstructs or weakens the overlap of the platinum d orbitals and the VDZ ligand orbitals. However, without X-ray crystal data to elucidate the structure of the less hindered isomer, no conclusions will be drawn. What can be determined though, is that the VDZ-based approach gives the kinetic isomer while the catechol-based approach gives the thermodynamic isomer.

III.2 Electrochemistry

Shown in Figure III.4 is the cyclic voltammogram of the VDZ-Pt-CAT complex. The data were obtained using THF as the solvent and tetra-*n*-butylammonium hexafluorophosphate (100 mM) as the electrolyte. The data shows two reversible redox waves at -0.78 V and -0.03 V versus ferrocene/ferrocenium. There is a third couple near +1.4 V which is irreversible, but it is at the end of the THF solvent window and could not be measured accurately. Other solvents were evaluated but THF gave superior results. This irreversible couple is likely the [VDZ-Pt-

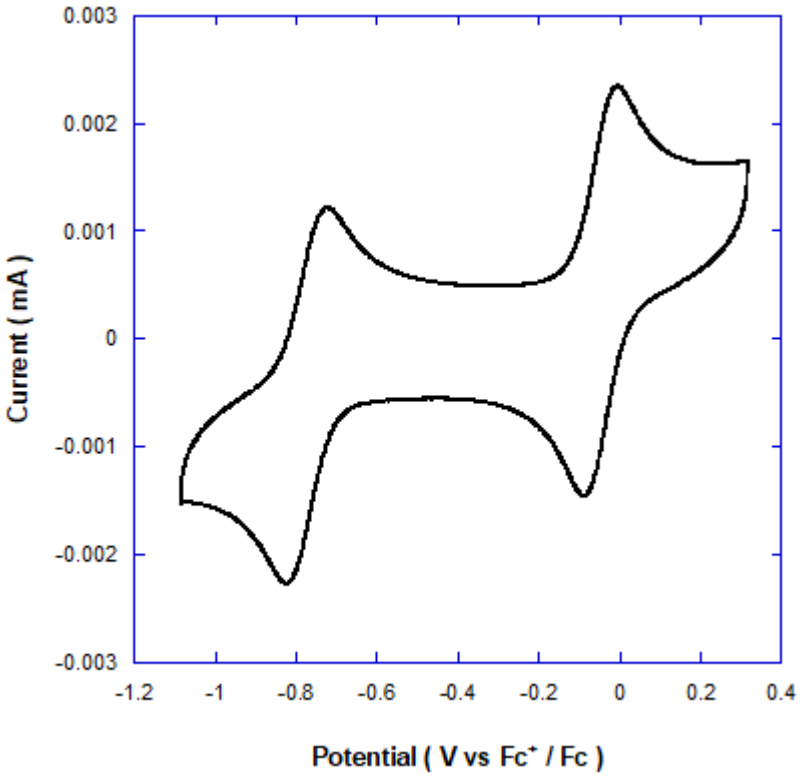

Figure III.4: Cyclic Voltammogram of VDZ-Pt-CAT in THF versus Fc^{+}/Fc.

$SQ]^{+}$ to $[VDZ\text{-}Pt\text{-}Quinone]^{+2}$ oxidation. Upon oxidation to the quinone, the quinone is expected to undergo decomplexation from the platinum center. The two reversible waveforms in the voltammogram and the redox couples they represent are shown in Figure III.5. The couple at -0.78 V represents the reversible reduction of the VDZ-Pt-CAT which involves the addition of an electron to the VDZ SOMO and the electrons are delocalized over the nitrogen of the tetrazane ring. The couple at -0.03 V is the reversible oxidation of the VDZ-Pt-CAT to $[VDZ\text{-}Pt\text{-}SQ]^{+}$. As shown in Figure III.5, the oxidation takes place predominantly on the CAT ligand and produces the corresponding semiquinone radical to give the $[VDZ\text{-}Pt\text{-}SQ]^{+}$ as a biradical complex with an overall positive charge. This process is reversible and the SQ complex is stable in the cyclic voltammetry experiment which was conducted under a nitrogen atmosphere at room temperature.

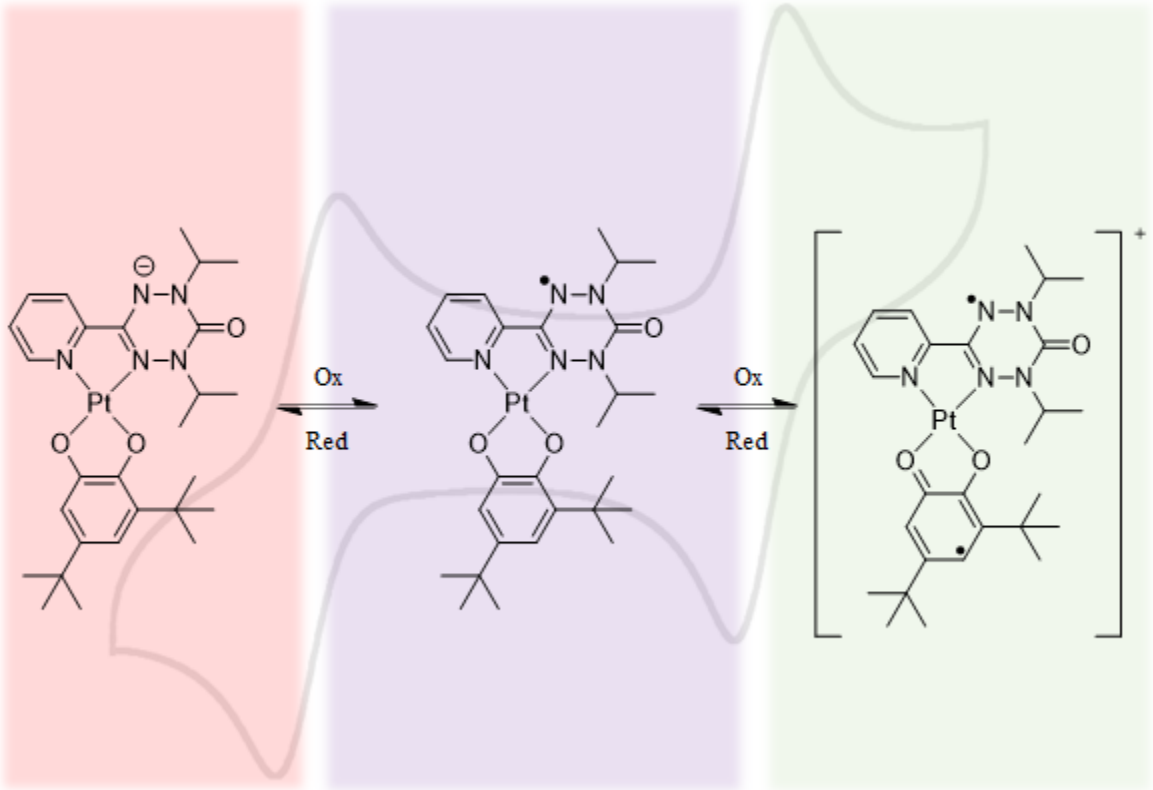

Figure III.5: Voltammogram couples.

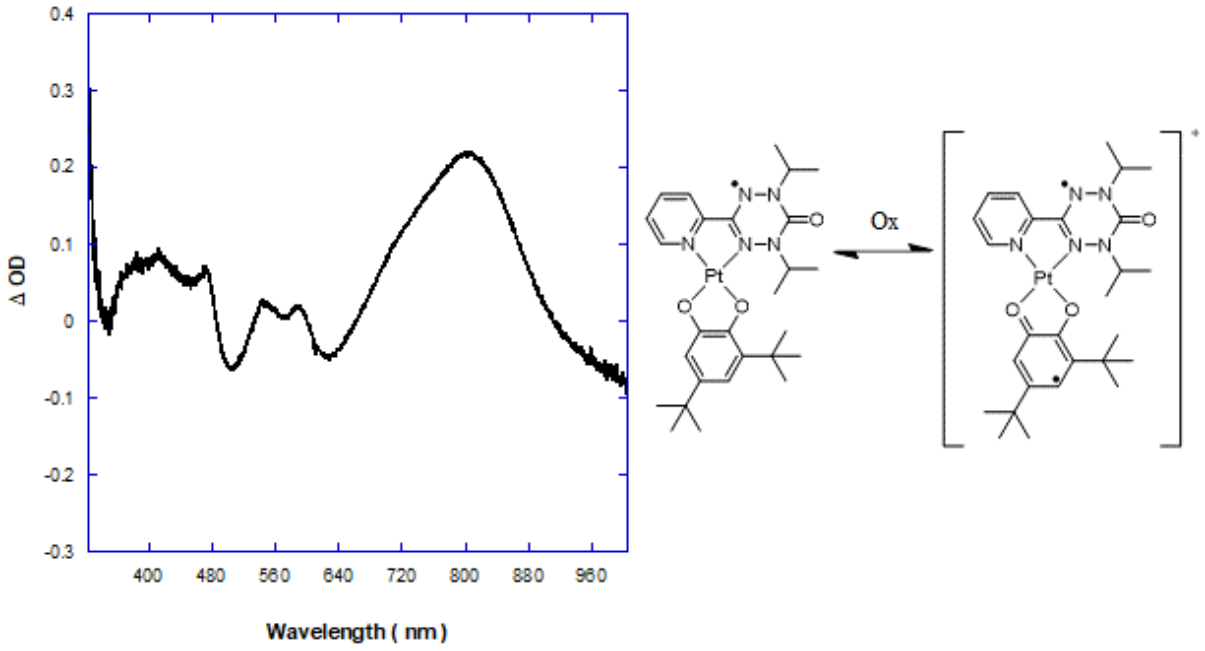

Figure III.6: Difference spectrum of the GS VDZ-Pt-CAT oxidation.

Given the results of the CV experiments, spectroelectrochemistry experiments were conducted with the VDZ-Pt-CAT complex. The difference spectrum obtained from the oxidation of the VDZ-Pt-CAT to $[VDZ\text{-}Pt\text{-}SQ]^+$ is shown in Figure III.6. The most obvious result is the broad and intense feature at 800 nm assigned to the SQ complex. One can see the ground state bleaching of the CAT → VDZ LL`CT band around 960 nm. The new feature at 800 nm is likely the SQ → VDZ LL`CT transition which is absent in the reduced form of VDZ-Pt-CAT. The blue shift of the SQ → VDZ LL'CT band compared to the CAT → VDZ transition is consistent with lowering the energy of the HOMO by one-electron oxidation.

III.3 Electron Paramagnetic Resonance

The electron paramagnetic resonance (EPR) spectra of the precursor free radical verdazyl, the VDZ-$PtCl_2$ and the VDZ-Pt-CAT complex provides valuable information concerning the electronic structure and spin distribution. The changes observed through the addition of the free verdazyl to $PtCl_2$ as well as the exchange of the ligands to form VDZ-Pt-CAT also provide a simple yet effective method for monitoring reaction progress with minimal interference from by-products.

In Figure III.6, the uncoordinated VDZ ligand is shown with a 9-line ^{14}N-hyperfine pattern. The expected, or theoretical, spectrum would be 25 lines when considering the 2NI+1 rule where I is the nuclear spin and N is the number of equivalent nuclei. There are two sets of two equivalent nitrogen nuclei in uncoordinated VDZ and ^{14}N is the isotope with the greatest abundance. The spin of ^{14}N is 1 which would give 2*2*1+1=5 for each set to yield 25 lines (pentet of pentets) in the spectrum. However, it is documented that the EPR spectra of the verdazyl class of radicals can give complex results due to the similar magnitude of hyperfine constants and the hyperfine interactions among the two sets of equivalent nitrogens and protons

from the substituent groups which are isopropyls in this case.[1,3] Among these results are cases

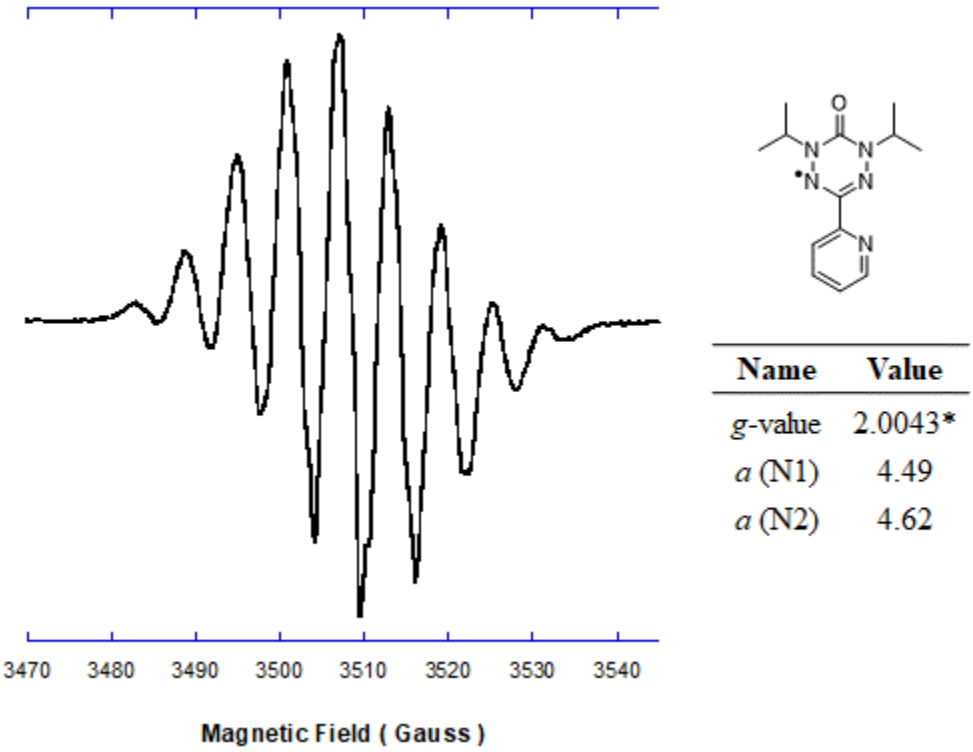

Figure III.7: EPR spectrum of uncoordinated VDZ with hyperfine constants (simulated) and g value (*literature[1]).

like that of the VDZ shown in this work where there are multiple overlapping lines but the line width is too great to observe all the hyperfine splitting which results in the simplified 9-line ^{14}N-hyperfine pattern as in this case.[1,3,4] However, closer inspection of Figure III.6 will show that some of the lines do have partially-obscured features within the broader lines. The peaks in the spectrum have spacings of approximately 4.5-5 Gauss and each of the nine lines maintain the same separation. The VDZ has a spin-only g-value of 2.0043,[1] characteristic of organic radicals comprised of light elements.

Following complexation to the platinum metal center, there is a dramatic change in the EPR spectrum as shown in Figure III.8. There are only two distinct features on the low-field side and very little resolved hyperfine structure. These peaks have a separation of about 25 Gauss and

can be attributed to the spin interactions of the platinum nucleus and the ^{14}N nuclei of the VDZ. The most abundant isotope, as well as the only spin active isotope of platinum, is ^{195}Pt at 33.83 % with a spin of ½, and is the contributing isotope in the spectrum. The high field side of the spectrum has a complex multiplet at 3500 Gauss which is attributed to small amounts of uncoordinated VDZ. The g-value was determined to be 2.015 by reference to DPPH (g = 2.0036). Unlike the free VDZ, there are few features in terms of hyperfine structure. Most hyperfine structure is obscured by the intense and broad peaks between 3400 and 3500 Gauss. These features of the VDZ-$PtCl_2$ indicate a small amount of spin density on the platinum ion.[1] Comparisons of the spectral width with that of free VDZ also show a significant increase from approximately 60 Gauss in the VDZ to 125 Gauss in the VDZ-$PtCl_2$. This characterization as well as the characterization of the VDZ are both consistent with that in the literature.[1,3,4]

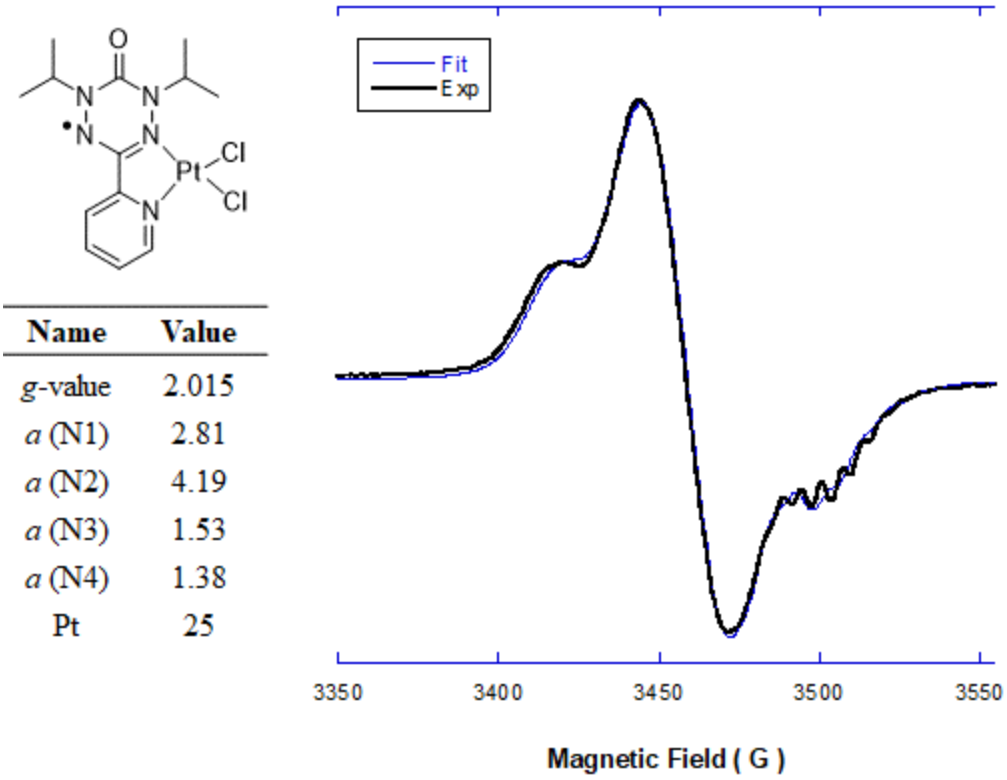

Name	Value
g-value	2.015
a (N1)	2.81
a (N2)	4.19
a (N3)	1.53
a (N4)	1.38
Pt	25

Figure III.8: EPR spectrum of VDZ-$PtCl_2$ and the hyperfine constants (*a*) in Gauss with the g-value.

Characterization of the title compound closely resembles that of the precursor platinum dichloride in that there is little in the way of hyperfine structure observed in the fluid solution as shown in Figure III.9. The most noticeable change is the platinum (^{195}Pt = 33.83%; I = ½) hyperfine nearly doubles from the 25 Gauss in VDZ-$PtCl_2$ to 43 Gauss in VDZ-Pt-CAT. There are now two distinct peaks in the low field side of the spectrum as opposed to the shoulder-like smaller peak in the VDZ-$PtCl_2$. The spectral width also increases from 125 Gauss to

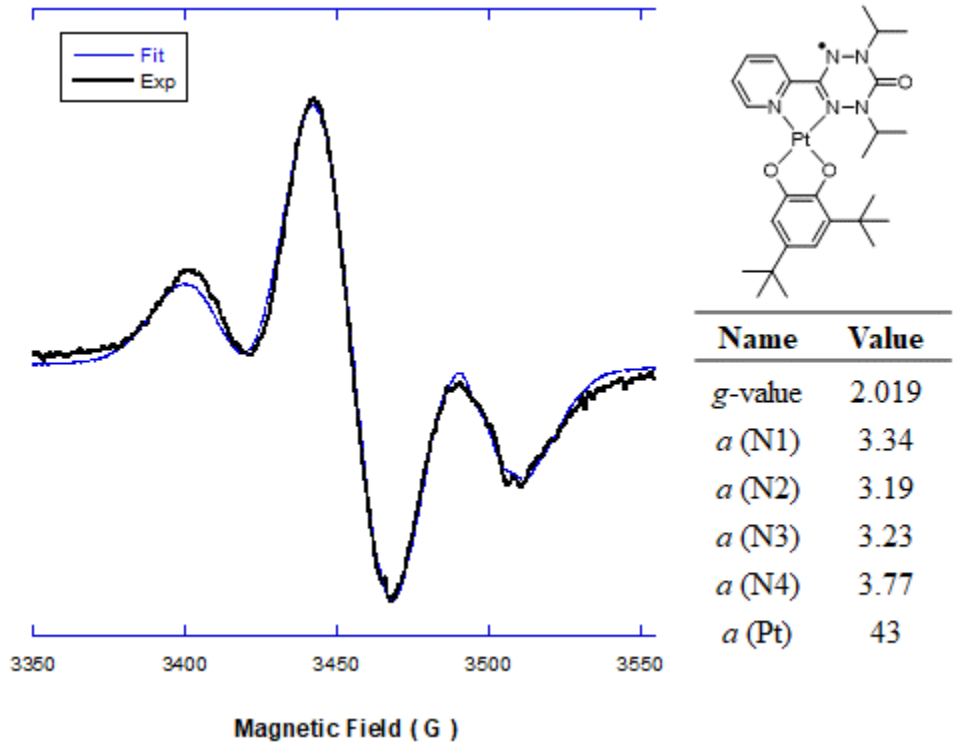

Name	Value
g-value	2.019
a (N1)	3.34
a (N2)	3.19
a (N3)	3.23
a (N4)	3.77
a (Pt)	43

Figure III.9: EPR spectrum of VDZ-Pt-CAT with g-value and hyperfine (in G) data.

approximately 175 Gauss which is almost three times the width of the uncoordinated VDZ (~60 Gauss). Hyperfine constants for the four nitrogens are very similar and range 3.19-3.77 Gauss. There is also a considerable increase in the g-values starting with 2.0043 for the VDZ which increases to 2.015 for the VDZ-$PtCl_2$ which increases further to 2.019 for the VDZ-Pt-CAT. With the most discernible features being the coupling to the I = ½ ^{195}Pt, there is a small amount of electron spin density on the platinum. Similar VDZ-$PdCl_2$ compounds have been shown in

literature to have EPR spectra with more verdazyl character with additional hyperfine features.[1] The g-values of the palladium compounds are also more in line with the free verdazyl in that

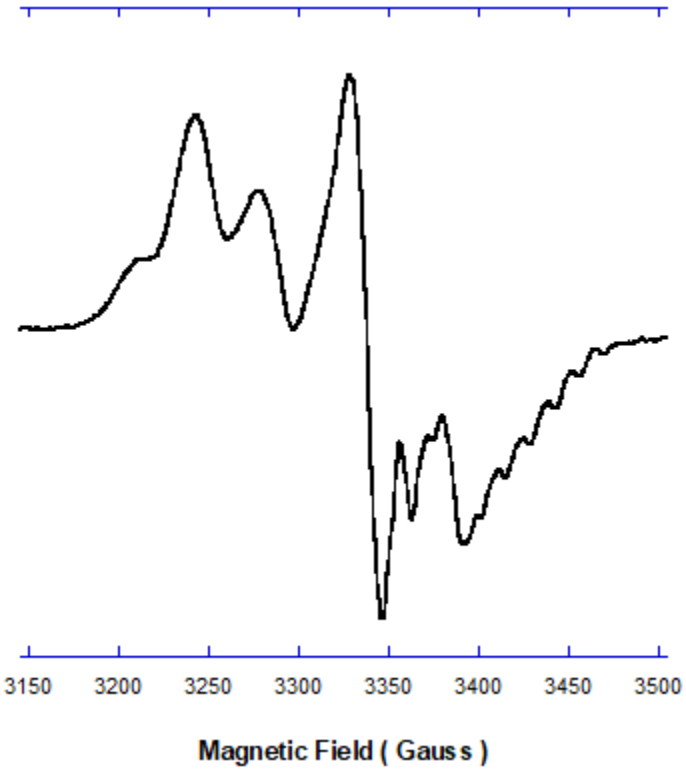

Figure III.10: Frozen solution EPR of VDZ-Pt-CAT at 100 K.

they ranged from 2.0065 to 2.0077.[1] By comparison, the VDZ-$PtCl_2$ and VDZ-Pt-CAT have values of 2.015 and 2.019, respectively. All of the presented data suggests that the ^{195}Pt ion may have an important role in the spin interactions of the VDZ-Pt-CAT complex.

III.3.A VDZ-Pt-SQ EPR Results

Oxidation of the VDZ-Pt-CAT to VDZ-Pt-SQ was attempted in efforts to form a biradical donor-acceptor complex. Shown in Figure III.11 **A** are results from the first attempt at oxidation using ferrocenium tetrafluoroborate. Notice how the spectral width is 450 G and the signal lacks intensity when compared to the baseline noise. Shown in Figure III.11 **B** are the results from a second oxidation attempt using identical conditions but at a later date. The

observed spectrum has a width of approximately 4200 G and has broad intense features which varies from the spectrum in Figure III.11 **A**. Upon observing two different results, a third oxidation was conducted the same day as the second ferrocenium oxidation with tris(4-bromophenyl)ammoniumyl hexachloroantimonate (magic blue) as the oxidizing agent while maintaining all other conditions the same as the previous attempts. This resulted in a spectrum that was identical to Figure III.11 **B**. To summarize, oxidation with ferrocenium tetrafluoroborate gave two different spectra while oxidation with magic blue gave a spectrum identical to one of the two previous attempts.

Comparing the spectra from Figure III.11 to the frozen solution spectrum of VDZ-Pt-CAT in Figure III.10 reveal that neither of the spectra are of the starting material. The spectrum

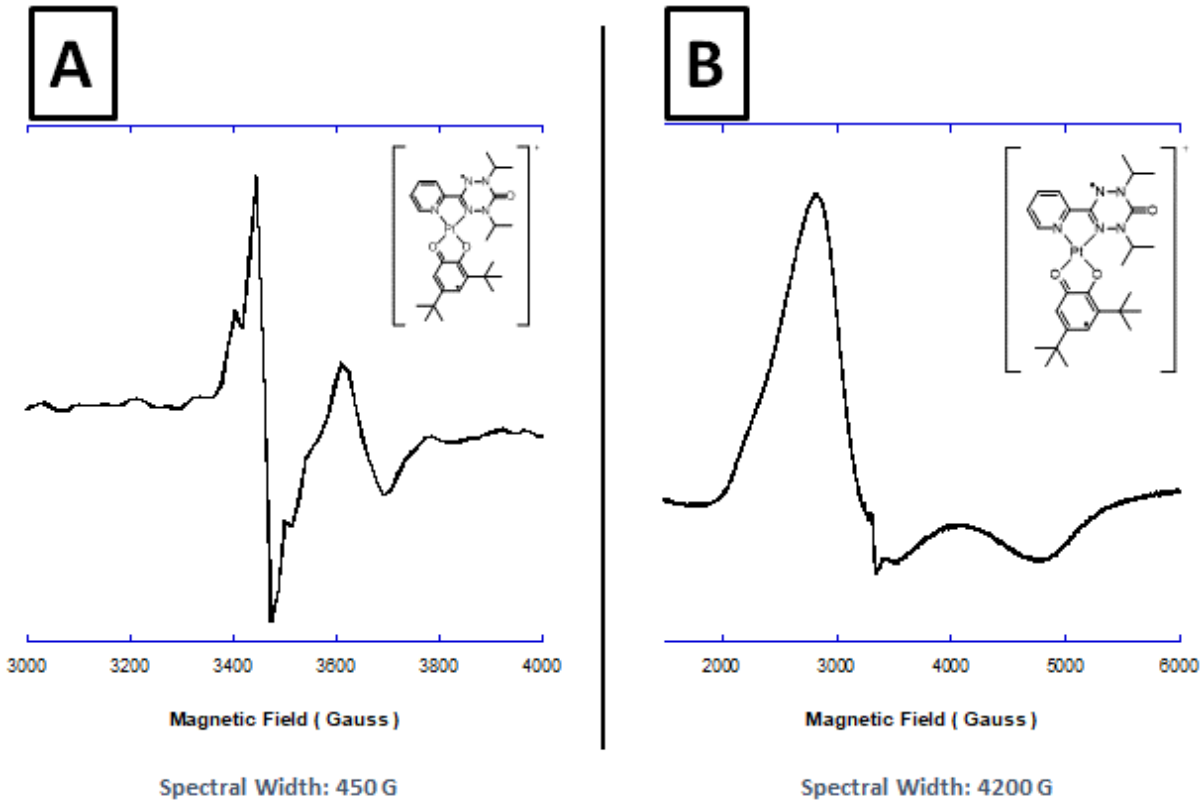

Figure III.11: A: Spectrum of the first oxidation attempt with ferrocenium. B: Spectrum that was observed for both ferrocenium and magic blue oxidations conducted at a later date.

of VDZ-Pt-CAT in Figure III.10 was collected using methyl THF which was the solvent that was used for the EPR experiments of all three oxidations. In addition, each of the three EPR experiments for the three oxidations were conducted in different EPR tubes at 110 K. The EPR signal for the oxidizers do not fall in the experimental range either. Considering everything, time was the only known factor to change from the first attempt to the second and third attempts. Other attempts to prepare $[VDZ\text{-}Pt\text{-}SQ]^+$ salts in the group have resulted in equally puzzling results. At this time, we hypothesize that the $[VDZ\text{-}Pt\text{-}SQ]^+$ complex may be a singlet ground state and that the EPR signals observed are merely impurities.

III.4 Conclusions and Future Work

Work detailing the design, synthesis and characterization of a Pt(II) donor-acceptor ground state analog with a charge-separated excited state has been presented. The design for the complex was based on Shultz group research while the VDZ ligand synthesis and early complexations were adapted from existing publications. While the synthesis of the VDZ ligand only required optimization, the complexation of the VDZ-Pt-CAT required rigorous testing of conditions and methods of purification. Reaction conditions for the synthesis of both coordination isomers were determined and characterization revealed the anticipated CAT → VDZ LL`CT excited state. The LL`CT transition was observable as a low-energy feature in the electronic absorption spectrum near 10,000 cm^{-1}. Cyclic voltammetry experiments revealed two redox couples. The couple at -0.7 V vs Fc/Fc^+ corresponds to the reversible reduction of VDZ-Pt-CAT which adds an electron to the VDZ SOMO while the couple at -0.03 V vs Fc/Fc^+ is from the reversible oxidation of VDZ-Pt-CAT to $[VDZ\text{-}Pt\text{-}SQ]^+$. Furthermore, spectroelectrochemistry experiments revealed what is believed to be the SQ → VDZ LL`CT transition of the $[VDZ\text{-}Pt\text{-}SQ]^+$. The EPR experiments exposed a spectrum with few features

other than the ^{195}Pt hyperfine of 43 Gauss and g-value of 2.019 with the broad features being indicative of some spin density on the Pt. Upon completion of the characterization of VDZ-Pt-CAT, attempts at oxidizing the complex to the biradical [VDZ-Pt-SQ]$^{+}$ yielded conflicting results. The two EPR spectra shown in Figure III.11 were both obtained running the same reaction conditions but vary significantly. It is hypothesized that the [VDZ-Pt-SQ]$^{+}$ may be in a singlet ground state which would mean that both spectra could be impurities. With the completion of the ground state analog, the next step would involve utilizing the work presented in section I.3. Namely, using a radical appended CAT donor (CAT-NN or CAT-IN) to form a charge-separated biradical capable of ground state ESP as is shown in Figure I.3. Using the research summarized in Figure I.4, it may be possible to control the singlet-triplet gap shown in Figure I.3 by synthetically altering the bridge (CAT-B-NN) of the donor. This would result in complexes unseen in the literature to date. Such complexes are highly advantageous to QIS and furthering our understanding of ultrafast optical generation, initiation and coupling of spin qubits. This next step would involve using previously synthesized and characterized CAT-B-NN donors instead of the CAT donor in the ground state analog presented. Synthetically, the changes to the procedure for VDZ-Pt-CAT would only involve changing the CAT ligand. However, due to the trouble encountered with the decomposition of VDZ-Pt-CAT, the synthesis could potentially face more problems than expected. Such outcomes would need to be taken into consideration. Regardless, the future possibilities for the VDZ-Pt-CAT ground state analog are highly anticipated.

III.5 References

(1) McKinnon, S. D. J.; Gilroy, J. B.; McDonald, R.; Patrick, B. O.; Hicks, R. G. Magnetostructural Studies of Palladium(Ii) and Platinum(Ii) Complexes of Verdazyl Radicals. *J. Mater. Chem.* **2011**, *21* (5), 1523–1530. https://doi.org/10.1039/c0jm02560g.

(2) Barclay, T. M.; Hicks, R. G.; Lemaire, M. T.; Thompson, L. K. Structure and Magnetic Properties of a Nickel(II) Complex of a Tridentate Verdazyl Radical: Strong Ferromagnetic Metal-Radical Exchange Coupling. *Chem. Commun.* **2000**, *212* (21), 2141–2142. https://doi.org/10.1039/b006520j.

(3) Koivisto, B. D.; Hicks, R. G. The Magnetochemistry of Verdazyl Radical-Based Materials. *Coord. Chem. Rev.* **2005**, *249* (23), 2612–2630. https://doi.org/10.1016/j.ccr.2005.03.012.

(4) Johnston, C. W.; McKinnon, S. D. J.; Patrick, B. O.; Hicks, R. G. The First "Kuhn Verdazyl" Ligand and Comparative Studies of Its PdCl2 Complex with Analogous 6-Oxoverdazyl Ligands. *Dalt. Trans.* **2013**, *42* (48), 16829–16836. https://doi.org/10.1039/c3dt52191e.

APPENDICES

Appendix A: Unsuccessful Attempts for pyrIN-Pt-CAT

A.1 Intent for pyrIN-Pt-CAT

Before the VDZ ligand was chosen, the pyridyl imino-nitroxide (pyrIN) was selected. Imino-nitroxides and nitronyl nitroxides are well-known in the literature and are often the stable organic radical of choice.[1] The Shultz group has also used these radicals for years with good

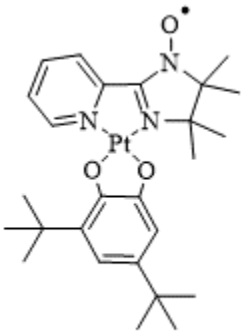

PyrIN-Pt-CAT

Figure A.1: pyrIN-Pt-CAT structure.

results. Therefore, the first attempts at a monoradical platinum (II) catecholate complex were with pyrIN as the ligand with the anticipated complex shown in Figure A.1. However, synthesis of this complex failed to meet the desired outcomes and resulted in the plans for this complex being shelved in favor of a different ligand. The results of the attempts at synthesizing pyrIN-Pt-CAT are discussed in this appendix.

A.2 Synthesis of the pyrIN Ligand

The synthesis of the pyrIN ligand is explored in literature and was prepared following existing procedures.[2–4] The synthetic scheme and yields are shown in Scheme A.1, while the

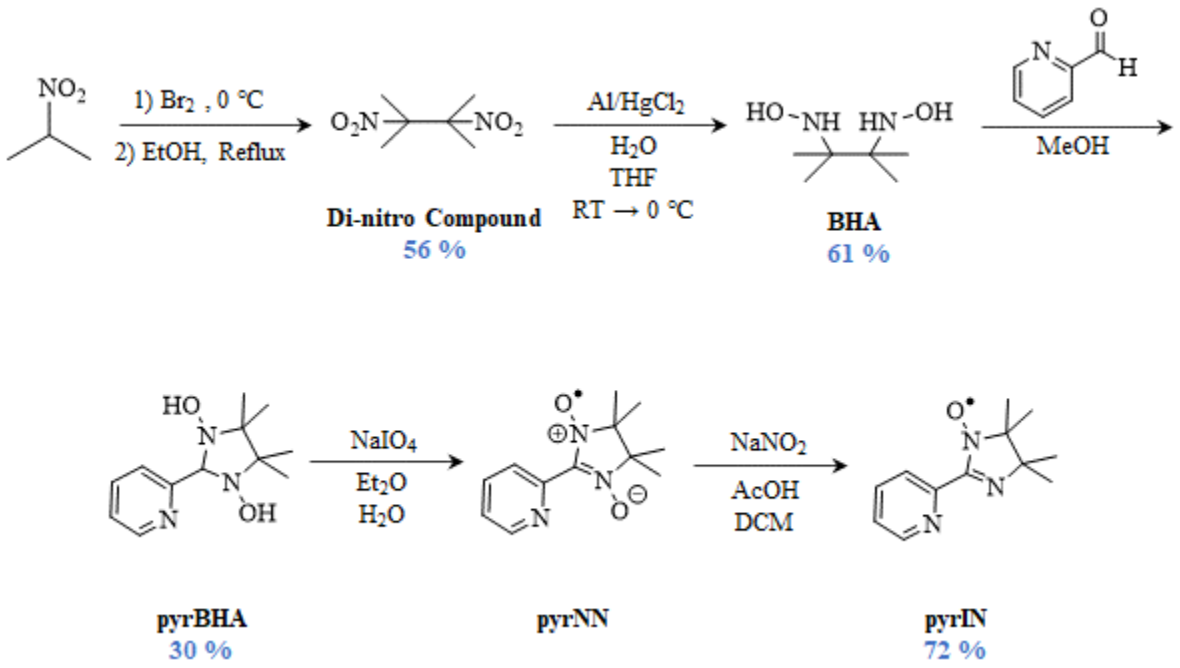

Scheme A.1: Synthetic route for the pyrIN ligand.

experimental procedures can be found in the experimental section. The reactions generally gave moderate yields and were easily purified through product precipitation or recrystallization which made the synthesis of the pyrIN a straightforward process.

A.3 The pyrIN-Pt-CAT Complex Attempts and Outcomes

Synthesis of the pyrIN-Pt-CAT complex began with Zeise`s salt and the pyrIN ligand in DMF. Zeise`s salt and the pyrIN were added to a reaction vessel and stirred for 24 hours in DMF. Upon completion, the reaction mixture was slowly added to H_2O and the precipitate was collected and allowed to dry under nitrogen to give pyrIN-$PtCl_2$ in good yields.

With the pyrIN-$PtCl_2$ collected, the next step was to coordinate the catecholate to give the final product shown in Scheme A.2. First attempts for this coordination involved potassium *tert*-butoxide as the base and DMSO as the solvent. This resulted in decomposition of the starting material as determined by EPR. The solvent was then switched to freshly distilled THF but still

resulted in decomposition. The stability of the pyrIN-$PtCl_2$ in the presence of base was then tested. Potassium *tert*-butoxide, cesium carbonate and triethylamine were all tested and gave decomposition of the radical. Following the decomposition results, this synthetic route was set aside in favor of a different approach shown in Scheme A.3.

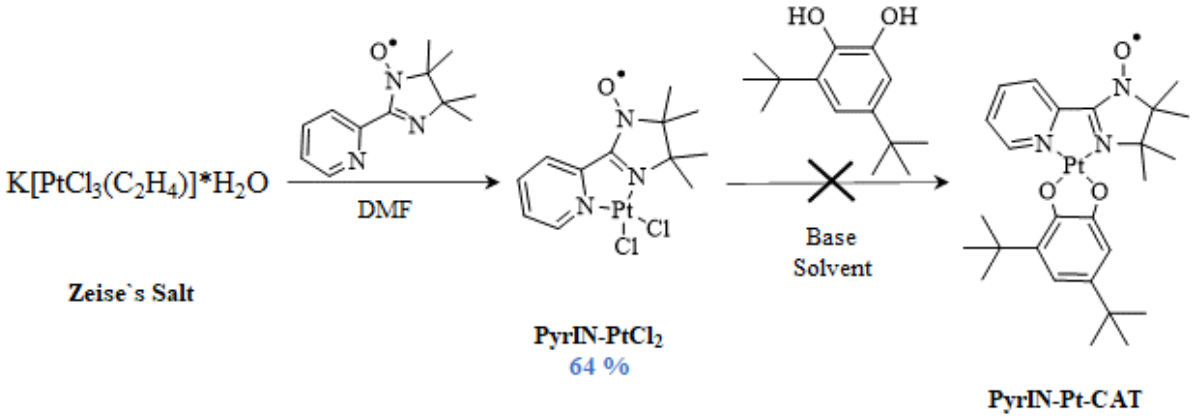

Scheme A.2: Synthetic scheme for pyrIN-Pt-CAT.

In a glovebox, sodium hydride and distilled THF were used to form the catecholate. This catecholate solution was then transferred to a vessel containing the pyrIN-$PtCl_2$ in distilled THF. However, this approach also resulted in decomposition of the radical. With the efforts to prevent excess base from interacting with the pyr-IN-$PtCl_2$ also not giving favorable results, it was decided that the addition of the catecholate ligand after the addition of the pyrIN ligand would

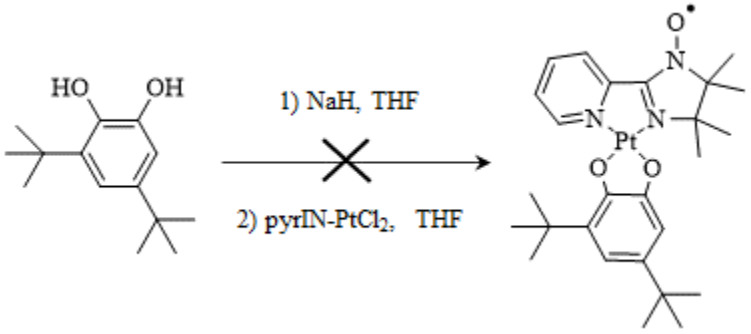

Scheme A.3: Synthetic approach using NaH.

not be feasible. A change in the sequence of ligand coordination could provide an alternate strategy but the decision to pursue a different ligand was made.

A.4 Experimental

2,3-dimethyl-2,3-dinitrobutane. 2-nitropropane (10 mL, 0.11 mol) and 6 M NaOH (23 mL) were added to a 100 mL round-bottom flask and cooled to 0 ℃. Bromine (2.8 mL, 0.056 mol) was added dropwise to the flask, followed by the addition of EtOH (20 mL). The reaction was heated to reflux overnight. It was then quenched by addition to chilled, stirring brine. The precipitate was collected, washed with H_2O and dried. Following recrystallization with MeOH, a colorless solid was obtained (5.54 g, 56 %). ^{1}H NMR (400 MHz, $CDCl_3$) δ = 1.65 (s, 12H). ^{13}C NMR (400 MHz, $CDCl_3$) δ = 22.0, 90.4. Data is consistent with literature.[2]

***N,N′*-(2,3-dimethylbutane-2,3-diyl)bis(hydroxylamine) (BHA)**. Aluminum foil (1.38 g, 0.051 mol) was cut into pieces and added to a 250 mL Erlenmeyer flask with enough H_2O to cover all the aluminum. Mercury(II) chloride (0.693 g, 0.0025 mol) was added with H_2O to the reaction vessel and stirred for 10 minutes until the solution became dark. The excess H_2O was decanted off followed by the amalgam being washed three times with 50 mL of H_2O, MeOH and then THF. A layer of THF was then added and the reaction cooled to 0 ℃. 2,3-dimethyl-2,3-dinitrobutane (1.50 g, 0.0085 mol) was then added with H_2O (3 mL). After 1 hour, the reaction was filtered through a pad of celite and washed with THF. The filtrate was then concentrated under reduced pressure to give a colorless solid. The product was then purified by recrystallization with EtOH to give **BHA** (0.768 g, 61 %). ^{1}H NMR (400 MHz, DMSO-d_6) δ = 1.19 (s, 12 H) ppm. MP: 181-183 ℃. Data is consistent with literature.[4]

2-(2-pyridinyl)-l,3-dihydroxy-4,4,5,5-tetramethylimidazolidine (pyrBHA). **BHA** (0.500 g, 0.0020 mol) was added to an oven-dried 50 mL round-bottom flask. The system was purged-pumped and put under nitrogen. 2-pyridinecarboxaldehyde (0.128 mL, 0.0014) and dry, deoxygenated MeOH (5 mL) were added and the solution was left stirring overnight. The precipitate was collected with vacuum filtration and washed with hexane and DCM to give the desired product **pyrBHA** (97 mg, 30 %). ^{1}H NMR (400 MHz, DMSO-d_6) δ = 8.48 (td, *J* = 0.8, 4.0 Hz, 1 H), 7.77 (dt, *J* = 1.8, 7.6 Hz, 1 H), 7.72 (s, 2 H), 7.61 (d, *J* = 7.8 Hz, 1 H), 7.28 (ddd, *J* = 1.2, 4.9, 7.4 Hz, 1 H), 4.65 (s, 1 H), 1.08 (d, *J* = 2.5 Hz, 12 H) ppm. ^{13}C NMR (400 MHz, DMSO-d_6) δ = 18.1, 24.3, 65.9, 92.1, 120.9, 122.3, 135.3, 147.8, 160.2 ppm. Data is consistent with literature.[3]

PyrIN. Sodium periodate (131 mg, 0.61 mmol) and **pyrBHA** (97 mg, 0.41 mmol) were added to a separatory funnel with diethyl ether (50 mL) and H_2O (50 mL) and shaken until purple and yellow layers formed (ca. 5 minutes). The organic layer was disposed of and the aqueous layer was extracted with DCM repeatedly until the aqueous layer was colorless. The extracted fractions were combined in a round-bottom flask. Sodium nitrite (84 mg, 1.2 mmol) and acetic acid (2 mL, 34.3 mmol) were added to the round-bottom flask and the reaction was left stirring under nitrogen for 24 hours. The reaction was then quenched with aqueous sodium bicarbonate and the organic layer was collected and dried with sodium sulfate. The solvent was removed under reduced pressure to give the desired product **pyrIN** (64 mg, 72 %). HRMS m/z: $[M]^+$ Theoretical for $C_{12}H_{16}N_3O$ 218.13251; Experimental 218.13522.

[(pyrIN)PtCl$_2$]. Potassium trichloro(ethylene)platinate(II) (76 mg, 0.19 mmol) and **pyrIN** (64 mg, 0.29 mmol) were added to a 50 mL round-bottom flask with DMF (10 mL). The reaction was left stirring for 24 hours. The reaction was then slowly added to H_2O and stirred for 10

minutes. The dark precipitate was then collected with vacuum filtration to give the title product (60 mg, 64 %). HRMS m/z: $[M]^-$ Theoretical for $C_{12}H_{16}Cl_2N_3OPt$ 483.03236; Experimental 483.03162.

A.5 References

(1) Borozdina, Y. B.; Mostovich, E. A.; Cong, P. T.; Postulka, L.; Wolf, B.; Lang, M.; Baumgarten, M. Spin-Dimer Networks: Engineering Tools to Adjust the Magnetic Interactions in Biradicals. *J. Mater. Chem. C* **2017**, *5* (35), 9053–9065. https://doi.org/10.1039/c7tc03357e.

(2) Do, H. Q.; Tran-Vu, H.; Daugulis, O. Copper-Catalyzed Homodimerization of Nitronates and Enolates under an Oxygen Atmosphere. *Organometallics* **2012**, *31* (22), 7816–7818. https://doi.org/10.1021/om300393m.

(3) Alcântara, A. F. d. C.; Piló-Veloso, D.; Stumpf, H. O.; De Almeida, W. B. NMR and Semiempirical Conformational Analysis of the 2-Aryl-1,3-Dihydroxy-4,4,5,5-Tetramethylimidazolidines. *Tetrahedron* **1997**, *53* (50), 16911–16922. https://doi.org/10.1016/S0040-4020(97)10145-4.

(4) Shimono, S.; Tamura, R.; Ikuma, N.; Takimoto, T.; Kawame, N.; Tamada, O.; Sakai, N.; Matsuura, H.; Yamauchi, J. Preparation and Characterization of New Chiral Nitronyl Nitroxides Bearing a Stereogenic Center in the Imidazolyl Framework. *J. Org. Chem.* **2004**, *69* (2), 475–481. https://doi.org/10.1021/jo0354443.

Appendix B: Difficulties with a Kuhn Verdazyl

B.1 Plans for a Kuhn Verdazyl as a Ligand

With the pyrIN-Pt-CAT complex not producing the desired outcomes, the idea to use a verdazyl in place of the pyrIN ligand was believed to be the best step forward. Literature has

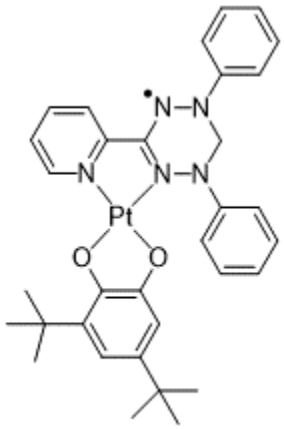

kVDZ-Pt-CAT

Figure B.1: kVDZ-Pt-CAT

shown that verdazyls can be robust ligands as well as have desirable properties for magnetic materials studies.[1,2] The Kuhn verdazyl (kVDZ) was chosen as it consisted of only three steps to form the completed ligand plus an additional two more steps to reach the desired kVDZ-Pt-CAT shown in Figure B.1. The reported yields for the formation of the pyr-formazan and subsequent oxidation to the kVDZ were low but within the tolerable limit given reagent prices and time saved when compared to the longer oxoverdazyl synthesis routes. Verdazyl reactions were also considered scalable which could help with blunting lower yields.[2] However, the synthesis of the kVDZ was plagued with inconsistent reaction results for the pyr-formazan and low yields of the kVDZ-$PtCl_2$.

B.2 Kuhn VDZ Ligand Synthesis Outcomes

Ligand synthesis began with the condensation of 2-pyridinecarboxaldehyde and phenylhydrazine. Reaction conditions consisted of stirring the aldehyde and hydrazine for 2 hours before collecting the yellow precipitate and washing with methanol. The results for this reaction were consistent with the reported yields and had favorable outcomes when being scaled up.

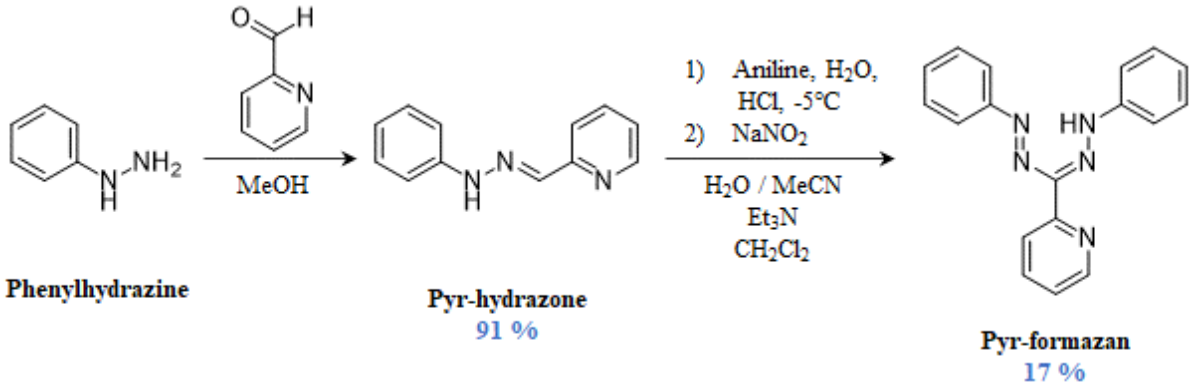

Scheme B.1: Reaction scheme from phenylhydrazine to pyr-formazan.

The second reaction shown in Scheme B.1 was both the most complicated reaction procedure-wise as well as the reaction with the most problems. The procedure involved forming a benzenediazonium salt from aniline and then adding this to a cold mixture consisting of triethylamine, pyr-hydrazone and chloroform. After stirring for an hour at -5 ℃, the reaction would then be worked up and purified. The problems were encountered in the formation of the benzenediazonium salt and the complications it had for purification.

Maintaining the conditions needed for diazonium salt formation was the greatest hurdle. This reaction needed to be done at -5 ℃ and anything above 5 ℃ would result in rapid

decomposition of the salt. However, water was used as one of the solvents and water freezes at 0 °C. The diazonium salt solution could not be cooled to anything below 1 °C as determined by a thermometer in solution. The solvent was changed to a 1 to 1 mixture of acetonitrile and water which resulted in a more favorable temperature of -2 to -1 °C. But to make the diazonium salt required adding a solution of $NaNO_2$ in water which would form nitrous acid when mixing with the aniline and HCl solution. This would cause the temperature to jump several degrees which is why a dropwise addition of $NaNO_2$ in water to the aniline solution is necessary. Anything faster than dropwise will raise the temperature above 5 °C and results in formation of copious amounts of brown precipitate. But if the addition is too slow, conditions for making a compound known as aniline yellow are reached and results in the formation of a yellow dye which complicates purification. These two reasons are responsible for the problems with the diazonium salt step.

The decomposition into the brown precipitate will completely kill the formation of the formazan but in the case of aniline yellow forming, the reaction can proceed. The yield will be lower but the real issue is trying to purify the crude product. The aniline yellow compound tends to cling to the product in columns of all conditions tested. Nevertheless, the reaction can be done but results in lower then anticipated yields with more than anticipated trouble.

With the pyr-formazan acquired, the next step involves the formation of the tetrazane ring structure with the consequent oxidation which is shown in Scheme B.2. Following the literature procedure,[3] the use of formaldehyde to form the tetrazane ring is followed up with oxidation to the kVDZ by exposure to oxygen in the atmosphere in a one pot procedure. To aid in the oxidation, oxygen was bubbled through the solution. Though still low yielding, bubbling pure oxygen through the reaction did increase the yield several percent higher then the reported literature yield.[3]

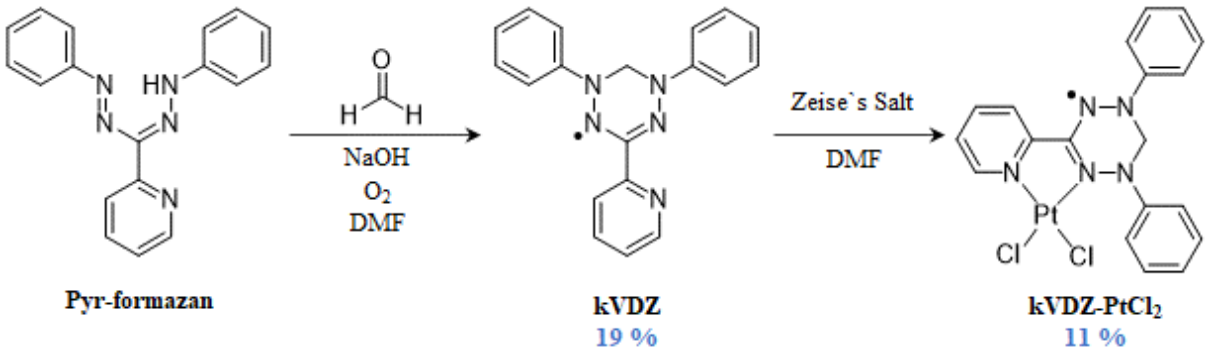

Scheme B.2: Synthetic route to kVDZ-$PtCl_2$.

The final step in Scheme B.2 which was ultimately the final step with this ligand is the coordination of the kVDZ to $K[PtCl_3(C_2H_4)]*H_2O$ (Zeise`s salt) to give kVDZ-$PtCl_2$. Stirring Zeise`s salt and the kVDZ in DMF for 2 hours followed by precipitation into water gave very poor yields of 11 %. These conditions were based off other work done in the Shultz group and not on any specific literature reference. There were no attempts at changing or optimizing these conditions due to the decision to shelve this ligand in favor of a different verdazyl ligand.

With a number of difficulties faced in the synthesis of the Kuhn verdazyl, this ligand was set aside in favor of a different verdazyl ligand. As shown, the synthesis up to kVDZ-$PtCl_2$ may have been difficult, but it was far from impossible. However, optimization of the reactions could range from minor changes to complete overhauls of the reaction conditions which would take significant time. Literature has already shown that Kuhn verdazyls are more prone to problems and lower yields when compared to their oxoverdazyl counterparts.[2] The Shultz group was seeking a ligand for expanded use in the future and choosing a ligand that has demonstrated unfavorable results at almost every step would be counterproductive in the long run. The possibilities for the synthesis of verdazyls are expanding every year with new methods and

synthetic routes.[4] While this ligand may be set aside for now, new breakthroughs could mean a new plan for the kVDZ as a ligand.

B.3 Experimental

Pyridine-2-carboxaldehyde-2′-pyridyl-hydrazone (pyr-hydrazone). Prepared according to literature procedure.[5] To a 100 mL round-bottom flask, 2-pyridinecarboxadlehyde (1.75 mL, 0.018 mol) and dry MeOH (30 mL) were added. Phenylhydrazine (1.82 mL, 0.018 mol) was added to the solution and the reaction was stirred for 2 hours. Upon completion, the yellow precipitate was collected with vacuum filtration and washed with MeOH to afford the desired product (3.31 g, 91 %). ^{1}H NMR (400 MHz, DMSO-d_6): δ = 10.67 (s, 1 H), 8.56 - 8.48 (m, 1 H), 7.97 - 7.87 (m, 2 H), 7.79 (m, 1 H), 7.30 - 7.21 (m, 3 H), 7.16 - 7.08 (m, 2 H), 6.85 - 6.77 (m, 1 H) ppm.

1-5-Diphenyl-3-(2-pyridyl)formazan (pyr-formazan). Adapted from literature procedure.[3] To a 50 mL round-bottom flask, H_2O (5 mL), MeCN (5 mL), aniline (0.25 mL, 0.0027 mol) and 12 M HCl (0.810 mL, 0.0097 mol) was added and the solution was cooled to -5 ℃. In a separate vessel, a solution of $NaNO_2$ (0.229 g, 0.0033 mol) and H_2O (2 mL) was made and then added dropwise to the aniline solution while maintaining -5 ℃ to form the benzenediazonium chloride. In a 100 mL round-bottom flask, a solution of 2-pyridinecarboxaldehyde phenylhydrazone (0.500 g, 0.0025 mol), triethylamine (0.705 mL, 0.0050 mol) and $CHCl_3$ (20 mL) was made and cooled to -5 ℃. The benzenediazonium salt solution was then added slowly and allowed to stir for 1 hour at -5 ℃ as the yellow solution gradually turned red. After completion, the reaction was transferred to a separatory funnel and the product was extracted using DCM. The organic layer was then washed with H_2O repeatedly until the aqueous layer would remain colorless. The organic layer was then dried with $MgSO_4$ and concentrated to a residue, followed by purification

by column chromatography using silica gel (Hexane-DCM-EtOAc, 7.5:2:0.5). The product afforded was a dark red solid (0.129 g, 17%). ^{1}H NMR (400 MHz, $CDCl_3$): δ =15.12 (s, 1H, NH), 13.22 (s, 1H, NH), 7.99 (ddd, 1H, J = 5.2, 2.5, 1.3 Hz), 8.71 (ddd, 1H, J = 5.7, 2.8, 1.2 Hz), 8.27 (dt, 1H, J = 8.3, 1 Hz), 8.01 (dt, 1H, J = 8.3, 1 Hz), 7.63 (dd, 2H, J = 8.9, 2.7 Hz), 7.55 (td, 1H, J = 8.9, 2.6 Hz), 7.34 (td, 1H, J = 8.8, 2.1 Hz), 7.20 (dd, 4H, J = 8.3, 2.1 Hz), 7.03 (m, 15H), 6.61 (tt, 1H, J = 7.1, 2.3 Hz) ppm. 13C NMR (400 MHz, $CDCl_3$): δ 154.4, 152.4, 152.0, 147.5, 146.0, 145.6, 144.0, 143.6, 141.2, 136.4, 135.3, 127.7, 127.6, 127.3, 125.3, 123.5, 122.4, 122.3, 121.8, 121.6, 119.5, 117.9, 113.3 ppm. Data is consistent with literature.[3]

1-5-Diphenyl-3-(2-pyridyl)verdazyl (kVDZ). Adapted from literature procedure.[3] 1-5-Diphenyl-3-(2-pyridyl)formazan (120 mg, 0.398 mmol) was dissolved in DMF (10 mL) in a 50 mL round-bottom flask. A solution of 37% formaldehyde (0.7 mL, 9.15 mmol) was added and the solution was stirred for 1 hour. A solution of 2 M NaOH (0.7 mL, 1.39 mmol) was then added slowly and the reaction was left stirring for 24 hours while O_2 was bubbled through the reaction mixture. It was then poured into Et_2O, washed with H_2O, dried with $MgSO_4$ and concentrated to a residue under reduced pressure. The product was purified with column chromatography on silica gel (Hexane-DCM-Et_3N, 14:6:1) to afford a dark solid (24 mg, 19%). HRMS m/z: [M^+] Theoretical for $C_{19}H_{16}N_5$ 314.14430; Experimental 314.14023. MP: 80-83 °C. Data is consistent with literature.[3]

[1-5-Diphenyl-3-(2-pyridyl)verdazyl]platinum(II) chloride (kVDZ-$PtCl_2$). 1-5-Diphenyl-3-(2-pyridyl)verdazyl (24 mg, 0.076 mmol) and $K[(H_2C{=}CH_2)PtCl_3]{*}H_2O$ (19 mg, 0.050 mmol) were dissolved in DMF (1 mL) and allowed to stir for 2 hours. The reaction was then slowly added to H_2O to give a dark precipitate. The precipitate was then collected with vacuum filtration

to give a fine powder (3 mg, 11%). HRMS m/z: $[M-H]^-$ Theoretical for $C_{19}H_{16}Cl_2N_5Pt$ 578.03577; Experimental 578.03736.

B.4 References

(1) McKinnon, S. D. J.; Gilroy, J. B.; McDonald, R.; Patrick, B. O.; Hicks, R. G. Magnetostructural Studies of Palladium(Ii) and Platinum(Ii) Complexes of Verdazyl Radicals. *J. Mater. Chem.* **2011**, *21* (5), 1523–1530. https://doi.org/10.1039/c0jm02560g.

(2) Lipunova, G. N.; Fedorchenko, T. G.; Tsmokalyuk, A. N.; Chupakhin, O. N. Advances in Verdazyl Chemistry. *Russ. Chem. Bull.* **2020**, *69* (7), 1203–1222. https://doi.org/10.1007/s11172-020-2892-6.

(3) Johnston, C. W.; McKinnon, S. D. J.; Patrick, B. O.; Hicks, R. G. The First "Kuhn Verdazyl" Ligand and Comparative Studies of Its PdCl2 Complex with Analogous 6-Oxoverdazyl Ligands. *Dalt. Trans.* **2013**, *42* (48), 16829–16836. https://doi.org/10.1039/c3dt52191e.

(4) Fuller, R. O.; Taylor, M. R.; Duggin, M.; Bissember, A. C.; Canty, A. J.; Judd, M. M.; Cox, N.; Moggach, S. A.; Turner, G. F. Enhanced Synthesis of Oxo-Verdazyl Radicals Bearing Sterically-and Electronically-Diverse C3-Substituents. *Org. Biomol. Chem.* **2021**, *19* (46), 10120–10138. https://doi.org/10.1039/d1ob01946e.

(5) Wu, W.; Li, X. Le; Fan, X. H.; Yang, L. M. An Easy Route to N,N-Diarylhydrazines by Cu-Catalyzed Arylation of Pyridine-2-Carbaldehyde Hydrazones with Aryl Halides. *European J. Org. Chem.* **2013**, No. 5, 862–867. https://doi.org/10.1002/ejoc.201201445.